A Simulator for Solar Array Monitoring

by

Shwetang Peshin

A Thesis Presented in Partial Fulfillment
of the Requirements for the Degree
Master of Science

Approved July 2016 by the
Graduate Supervisory Committee:

Andreas Spanias, Co-Chair
Cihan Tepedelenlioglu, Co-Chair
Devarajan Srinivasan

ARIZONA STATE UNIVERSITY

August 2016

ABSTRACT

Utility scale solar energy is generated by photovoltaic (PV) cell arrays, which are often deployed in remote areas. A PV array monitoring system is considered where smart sensors are attached to the PV modules and transmit data to a monitoring station through wireless links. These smart monitoring devices may be used for fault detection and management of connection topologies. In this thesis, a compact hardware simulator of the smart PV array monitoring system is described. The voltage, current, irradiance, and temperature of each PV module are monitored and the status of each panel along with all data is transmitted to a mobile device. LabVIEW and Arduino board programs have been developed to display and visualize the monitoring data from all sensors. All data is saved on servers and mobile devices and desktops can easily access analytics from anywhere. Various PV array conditions including shading, faults, and loading are simulated and demonstrated.

Additionally, Electrical mismatch between modules in a PV array due to partial shading causes energy losses beyond the shaded module, as unshaded modules are forced to operate away from their maximum power point in order to compensate for the shading. An irradiance estimation algorithm is presented for use in a mismatch mitigation system. Irradiance is estimated using measurements of module voltage, current, and back surface temperature. These estimates may be used to optimize an array's electrical configuration and reduce the mismatch losses caused by partial shading. Propagation of error in the estimation is examined; it is found that accuracy is sufficient for use in the proposed mismatch mitigation application.

DEDICATION

To my parents.

ACKNOWLEDGMENTS

I wish to thank my advisors Prof. Andreas Spanias and Prof. Cihan Tepedelenlioglu for their constant support and evaluation of my work. Their technical expertise and insight helped me become a better researcher and complete this work. I am grateful to for taking the time to review my thesis and being a part of my committee.

I would also like to thank Ms. Toni Mengert for helping me with paperwork at all the different stages of my graduate studies.

I have received lot of assistance from my colleagues and friends in the SENSIP research group. Special thanks to my colleague and friend Jongmin Lee who was a constant support and for helping out in every way possible. I would also like to thank David, Henry, Sophia, Sai, Huan, Chinmay, Alan, Prasanna and Mahesh for providing assistance in times of need.

I am also extremely grateful to all my friends and family who have kindly provided me assistance and companionship in the course of preparing this thesis.

Finally, many thanks go to my parents for their unfailing love, unwavering support and sacrifice without which this would not have been possible.

TABLE OF CONTENTS

Page

CHAPTER Page

LIST OF TABLES

Table Page

LIST OF FIGURES

Figure Page

Chapter 1

INTRODUCTION

This chapter introduces the motivation behind the topic of research and gives a general outline of photovoltaic (PV) systems). The contribution and organization of the thesis is also briefly discussed.

Alternative renewable energy sources have been gradually replacing existing ones. One of the most promising alternate energy sources is solar which is becoming increasingly more efficient and cheaper to install. With emerging solar technologies, experts calculated that the average energy derived from solar radiation can provide up to 10,000 times more than the world's current needs [1]. In many countries, generation of electricity based on solar energy, especially photovoltaic (PV) cells, is being promoted with incentives for utility scale energy generation. The global solar PV market has been growing with almost half of all PV capacity added in the past two years, and approximately 98% of current systems have been installed since the beginning of 2004 [2]. PV modules produce no greenhouse gasses during operation and relatively little during manufacturing, and do not require significant resources which must be imported from other countries. There are no complicated moving parts associated with the PV power generation. This results in a very low operating cost and maintenance. Also it is freely available and abundant in nature.

In spite of the several advantages, PV technology faces various barriers which prevent its wide deployment. The major barrier is the initial cost of setup. In the US as of 2010, the average cost of solar energy was $211/MWh, while it was $95/MWh for coal

generated power [3]. Also, solar arrays are low efficiency compared to the light incident on them. Performance analysis of a 342kW roof mounted PV array using 10 years of data showed the array operating with an efficiency of 7-9 percent [4]. Thus, to improve PV array output is to ensure that the array operates in optimal output conditions at all times. PV arrays once installed are expected to operate with minimal human intervention. Despite the fact that solar PV systems have no moving parts and usually require low maintenance, they are still subject to various failures or faults along the PV arrays, power conditioning units, batteries, wiring, and utility interconnections [5, 6]. Most of these faults remain undetected for long periods of time resulting in loss of power. This results in reduced uptime of the array and decreased PV efficiency. The energy generation is often affected by conditions such as irradiance, temperature (weather conditions) and the connection topology of the PV array, which determine its overall power output [7]. In order to improve power generation robustness and predict system conditions, fault detection and monitoring [8-11] methods have been proposed.

Especially for PV arrays, it is difficult to shut down PV modules completely during faults, since they are energized by sunlight in daytime. Once PV modules are electrically connected, any fault among them can affect the entire system performance. This means the PV system is only as robust as its weakest link (e.g., the faulted PV components). In a large PV array, it may become difficult to properly detect or identify a fault, which can remain hidden in the PV system until the whole system breaks down. Due to the widely distributed PV arrays and the massive amount of generated sensor data, acquisition, storage and analysis in the monitoring processes is also a problem. By replacing current ad-hoc methods of monitoring and fault detection, the efficiency of PV arrays may be

increased while decreasing the net cost of electricity from PV sources. Current methods of fault detection are not reliable, are slow with more than 3 days of turnaround time, and rely on manual monitoring by technicians [12].

In most cases, remote facilities using manual monitoring methods such as panel by panel manual metering which is very time consuming [13]. This is prone to errors and takes a lot of resources and manpower for completion. Thus, PV array monitoring systems need to be automated for the processes of data monitoring, acquisition and storage. The family of technologies and protocols collectively known as the smart grid (smart PV array) offer an opportunity to change this: with increased monitoring and communication among PV array components, significant improvements in overall array power production may be achieved.

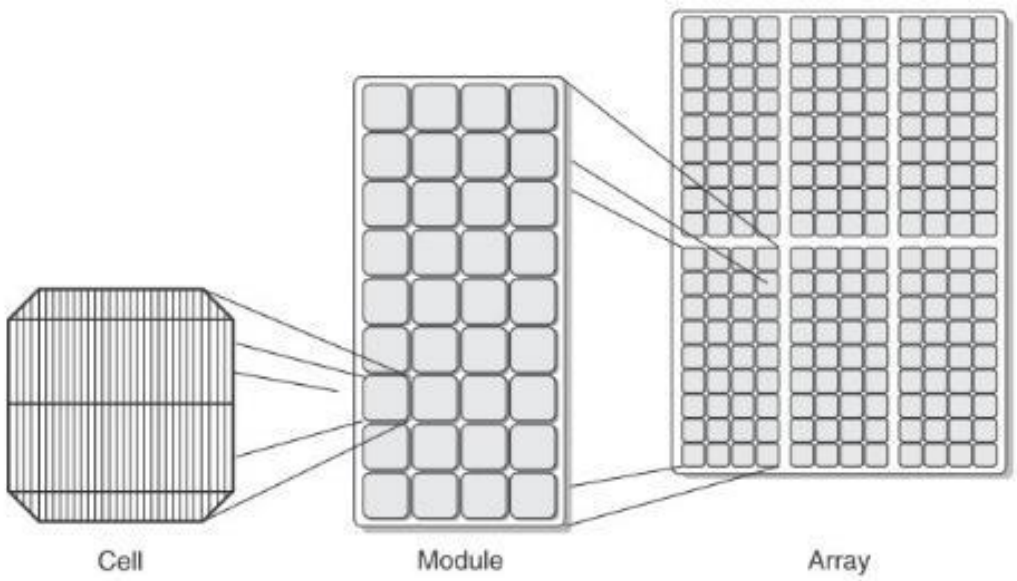

Figure 1.1 Photovoltaic Cells, Modules and Arrays.[141]

Single Diode Model and I-V Characteristics

PV arrays convert solar radiation incident on them to electricity. They are composed of several components such as PV modules, inverters and electrical connections. The block diagram of a typical PV array is shown in Figure 1.1. Furthermore, PV is scalable and modular technology that can build a PV power plant by connecting a large number of PV modules in series and parallel configuration. PV modules in the same row are connected electrically in series to increase the generated voltage. This series arrangement is called a string. To form the array, several strings are connected in parallel thereby increasing the current generated. The DC power generated by the array is converted to AC by means of an inverter.

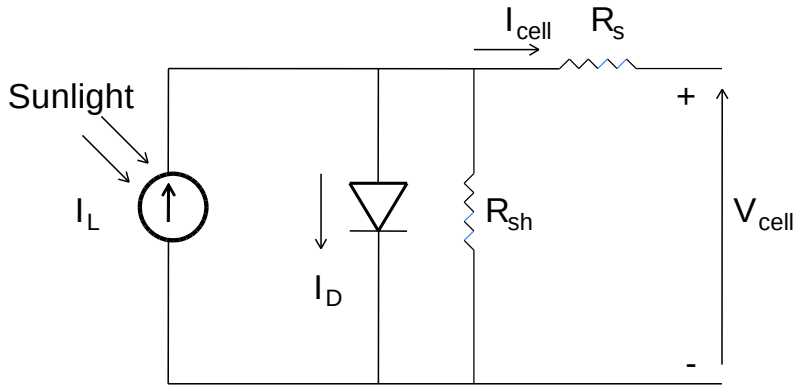

Figure 1.2 Single-Diode Model of a PV Module.

The output current and voltage of a solar module depends on several factors such as module temperature, irradiance (amount of solar radiation power incident per square area), angle of incidence of the sun and spectrum of the incoming light [14–16]. A solar module is often modelled as a current source in parallel with a diode, with parasitic series and shunt resistance [17–19] as shown in Figure 1.2.

As with the diode, we can characterize the behavior of the PV module by its current-voltage relationship. I_L is the light generated current and it depends mainly on the irradiance. Hence the PV module generates more current at higher irradiance values. The voltage across the diode depends mainly on the module temperature and the PV module outputs higher voltage at lower temperatures. The current voltage (I-V) characteristics of a PV module operating at standard test conditions of 1000 W/m^2 irradiance and 25 degrees' Celsius temperature is shown in Figure 1.3. V_{OC} and I_{SC} represent the open circuit and the short circuit conditions respectively. For a given set of environmental conditions, the solar module has a voltage and current (V_{MP}; I_{MP}), at which it produces its maximum power P_{MP}. Modern inverters dynamically adjust the load they present to a solar array in order to maintain operation near P_{MP} using a process known as maximum power point tracking (MPPT) [20–23].

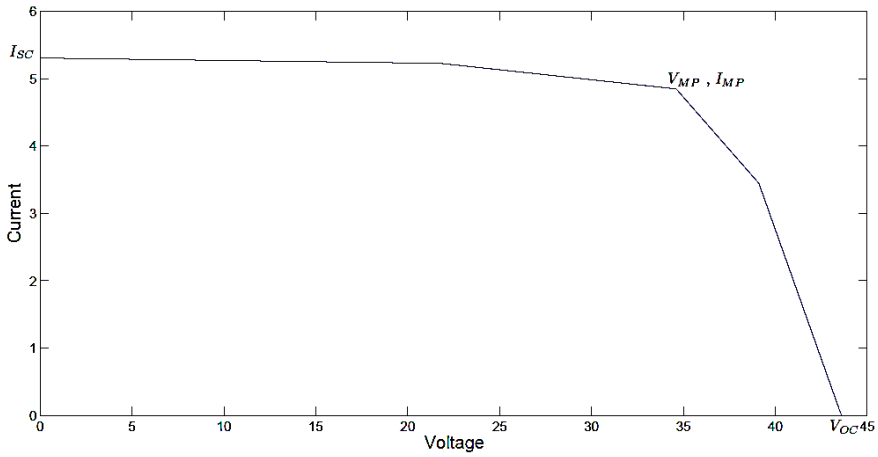

Figure 1.3 I-V Curve of a PV Module at Standard Test Conditions.

For an ideal PV array, the power output is the sum of the power generated by each of the modules. However, PV array performance can be reduced significantly in the

presence of faults. Several types of faults such as module mismatch [24], soiling [25], shading [26–28], ground faults [29] and arc faults [30, 31] occur in PV arrays. The series-parallel topology commonly employed in PV arrays implies that every module in a string must carry the same current. As a result, faults in a single module would result in a sub-optimal operating point for all the modules in a string, leading to a higher loss of power. For instance, it is shown in [32] that a partial shadow on a single string can result in a loss of power corresponding to over 30 times its physical size. Hence, any fault in the array must be identified as soon as possible. Due to faults occurring within PV arrays, several fire hazards have been reported in PV installations [33, 34]. Fig. 1.4 shows the results of a fire hazard in a 383 kW PV array in Bakersfield, California in 2009.

Figure 1.4 Fire Hazard in a 383 kW PV Array in Bakersfield, California in 2009. [34]

In these cases, the fault remained unnoticed and hidden in the system until the hazard caused catastrophic fire. These fire hazards not only show the weakness in conventional fault detection and protection schemes in PV arrays, but also reveal the urgent need of a better way to prevent such issues. Faults such as shading of a few modules within the array cannot be detected from the AC side. Parameters to measure on

the DC side include DC voltage and current at the inverter, string/module voltages and currents and module temperatures.

The next topic considered is irradiance estimation for overall cost reduction for the PV array setup, monitoring and fault mitigation. A method is presented here for estimating the circuit parameters of partially shaded PV arrays given measurements from the smart PV array is shown in Fig1.5 described above.

(a) First Generation Installed on Array (b) Current Generation

Figure 1.5 Prototype Monitoring Devices.

This method is intended as a step toward a comprehensive mismatch mitigation strategy, in which switching or load matching is used to allow PV modules to operate near their maximum power point (MPP) even under mismatch conditions. One potential approach to this mismatch mitigation problem requires an accurate circuit model of the PV array, in order to perform simulations and determine the optimal configuration [35–37]. Since the behavior of PV modules depends on environmental conditions, this

requires knowledge of incoming irradiance and module temperature, at a minimum. However, at the time of this writing, reasonably accurate pyranometers are far too costly for installation of many irradiance sensors within the array. Temperature, current, and voltage sensors are much more affordable and may feasibly be deployed at the module level.

The method presented here may be viewed as a way to use an operating PV Cell as its own pyranometer, deriving an accurate circuit model for analysis and simulation without relying on expensive direct measurements of irradiance. A small body of previous work on estimation in PV arrays is available. For instance, in [38] voltage and current measurements are used to estimate PV cell temperature. While useful, this method rests on the assumption that a module is operating at its maximum power point; under the partial shading conditions we wish to consider, this assumption is not valid.

This work tries to address two of these factors. The monitoring and visualization of data is studied using a LabVIEW GUI built for a small scale PV array as well as cost reduction using estimation techniques.

1.1 Problem Statement

A series of articles have reported different monitoring systems [39-40] which, however, have been for the most part expensive and somewhat difficult to manage. In [39], data communications have been provided by cables which results in increased implementation cost and in [40] power line communications are incorporated which limit the transmission data rate. From previous studies, it was shown that around one fifth of

the total operational failures in PV array systems [41] are due to faults in PV modules which can be remedied by a monitoring system.

First, we present a simulator of a smart PV monitoring system that is easy to manage and low-cost. Our simulator is implemented with LABVIEW GUI [42] and an Arduino Uno board. The group at Arizona State University has previously created several LabVIEW GUI and smartphone simulations [43] for signal analysis as well theory and award winning apps for Digital Signal Processing [44]. This system though is different in that actual solar and sensor hardware is interfaced to an Android app via an Arduino board. Thus, system can be accessed via the Internet using a browser or an app running on mobile devices for obtaining the latest monitoring status. This system is built for demonstration purposes. The simulator has been placed in a controlled- environment to test the performance of the entire system similar to [45]. We demonstrate that the simulator can be used to measure current, voltage, irradiance, and temperature to detect and deal with partial shading, ground fault, or other conditions which can cause reduction in power output [46, 47].

And secondly, we consider the problem of deriving a circuit model of a PV array under partial shading conditions, using only voltage, current, and temperature measurements from every module. Several factors complicate this task and make it non-trivial. Since measurements are taken on an active and functioning array, I-V curves from individual modules are not available. Also, since partial shading is present, we can no longer assume that module-level measurements are taken at the modules' maximum power point (MPP). This is because an inverter with maximum power point tracking

(MPPT) will seek the array's maximum power point, causing some or all of the modules to operate away from their own MPP. Finally, shading affects not only the power of the incoming solar radiation, but its spectrum as well. Air mass models exist to predict the effect of changing solar spectral characteristics [48], but these typically assume light travels through clear, dry air.

1.2 Contributions

The contributions of this research can be summarized as follows:

- Design of hardware for the PV array monitoring simulator and software for visualization of module level voltage and current
- Simulation analysis and understanding of shading, faults and loading on a small scale PV array system
- Algorithm presented which accurately estimates circuit parameters i.e. irradiance when air mass and cell temperature are known and measurements are accurate,

1.3 Thesis Organization

This thesis is organized as follows. Chapter 2 describes earlier study and research in areas of fault detection, array optimization and monitoring for the PV arrays. Chapter 3 talks about the design and working of PV monitoring simulator including the software and hardware design of the system. Chapter 4 talks about the irradiance estimation procedure and sources of error are also discussed. Chapter 5 presents the experimental results and simulation analysis. And, the thesis document ends with a final chapter of conclusions and future work.

Chapter 2

EXISTING METHODOLOGIES – A LITERATURE REVIEW

The following literature review discusses the advances in the field of solar array monitoring, fault detection and optimization. The importance to make solar energy a viable and cheap source of power has caused a recent surge of interest from researchers and commercial institutions alike, in these areas. The review involves literature revolving around research and development done in the area of solar array monitoring, Fault Detection and topology optimization area in recent years with focus on some crucial and key papers. Accordingly, journals and papers were identified which were relevant and contributed to the progress in the fields according to their relevance and importance. The review is divided into three main sections which focus on fault detection methods, PV array Topology optimizations and monitoring of PV systems.

2.1 Fault Detection Methods

Fault detection is very crucial for the optimal operation of the PV arrays. There has been a spike in interest in this area as it can improve overall power production and maintenance cost by quite a margin. There are various methods to the fault detection in PV array.

2.1.1 Model-based Methods

One of the basic approaches to detect unexpected power loss is comparing the output with a reference value and trigger an alarm when significant differences are detected while monitoring. The approach taken in [49] is to perform monitoring using

satellites, essentially building up known weather conditions. This approach is not applicable to this study due to insufficient weather data available. An extension of this method is building an analytical model [50-52] based on the one-diode model introduced in chapter 1. This method relies on access to both irradiance and solar panel temperature measurements in order to calculate the reference MPP. This is then compared to the measured working point as previously discussed. An active approach is described in [53], where the whole I-V curve is studied for defects, and the maximum attainable V_{max} and I_{max} are recorded over time. Due to the nature of sweeping I-V curves this implies that this gives a reduction in power output during the analysis. In addition, it is not applicable to passive studies of systems since they can be assumed to deliver output at the MPP. Two studies by Vergura et al. [54, 55] consider several identical PV strings and compare the outputs in order to classify significant deviations. This is done by checking if certain statistical assumptions can be made, formally that the power differences are independently normally distributed with identical variance. If this is the case, a method known as analysis of variance (ANOVA) [55] can be applied in order to build confidence interval for the power output of each PV string. Otherwise the Kurskal-Wallis test [55] is applied in order to build the corresponding intervals. The resulting confidence intervals can be studied for significant deviations which would imply defect solar modules.

Current-Voltage (I-V) Analysis

Current vs. voltage (I-V) curve analysis can provide most of the operating points of a PV module, string or array. As illustrated in Fig. 2.1, the I-V curve reveals salient PV characteristics. Therefore, it is possible to detect and classify PV faults, such as series

losses, shunt losses, mismatch losses, reduced current and reduced voltage based on I-V characteristics [56-59].

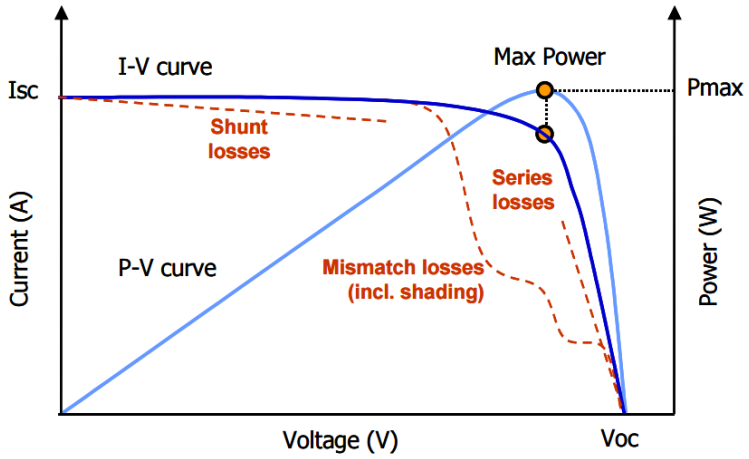

Figure 2.1 I-V Curve Reveals Salient PV Characteristics.[142]

Performance Comparison

In addition to fire hazards and safety issues, faults in PV systems may cause a large amount of energy loss. Therefore, it is necessary to monitor PV system performance, study the fault pattern and develop the fault detection methods. Performance comparison compares the actual PV performance with the simulated performance under real-time operation [57, 60]. Recently, performance comparison has been proposed for fault detection. Generally, it compares the actual performance with the expected performance. The fault detection rule is straightforward: significant difference in produced and measured output performance may indicate a fault. The performance evaluation usually has several components, including weather information such as solar irradiance and temperature, expected PV performance as a benchmark, actual measured PV performance, performance comparison and fault detection. For example, to prevent

energy and subsequent financial losses in PV systems, an automatic PV performance comparison has been proposed in [60], which monitors the difference between the simulated and actual energy yield in real time. The fault detection system gathers satellite-derived solar irradiance and ambient temperature, which are fed into the simulation model to predict the PV's AC output power (P_{sim}). Meanwhile, it monitors the actual AC output power (P_{actual}) and compares it with (P_{sim}). Four general fault categories are: Constant energy loss, changing energy loss, snow cover and total blackout. The limitation exists: since it monitors the PV power over a period of time (equivalent to energy yield), it has a slow response. For example, this fault detection method may take at least one day.

Performance Ratio (PR) Method

Performance ratio (PR) is proposed in [61, 62] as a normalized parameter of the PV system energy yield to evaluate the system performance. Independent of the orientation and inclination of the panel, PR considers the overall effects of system losses so that it can be used for fault detection. It is usually defined in equation below (2.1) using the final yield (Y_f) over the reference yield (Y_r).

$$\mathrm{PR} = \frac{Y_f}{Y_r}\ (\text{dimensionless}) \tag{1}$$

Specifically, Y_f represents the normalized AC energy output to the utility grid. It is defined in (2.2), where E is the net AC power output and P_0 is the nominal PV power.

$$Y_f = \frac{E}{P_0}\left(\frac{kWh}{kW}\right) or\ (hours) \tag{2}$$

On the other side, Y_r represents the normalized solar irradiation conditions. It is defined in (2.3), where H is the total in-plane solar irradiation (kWh/m^2) and G_{STC} is 1 kW/m2.

$$Y_f = \frac{H}{G_{STC}} \ (hours) \tag{3}$$

PR values for PV systems are commonly reported on a monthly or yearly (long-term) basis. For short-term basis, such as daily or weekly, PR gives better resolution and it can be used for fault detection in PV systems. For instance, as shown in Fig. 2.11, most of the PR values lie between 0.65 and 0.8 when the PV system is normally operating.

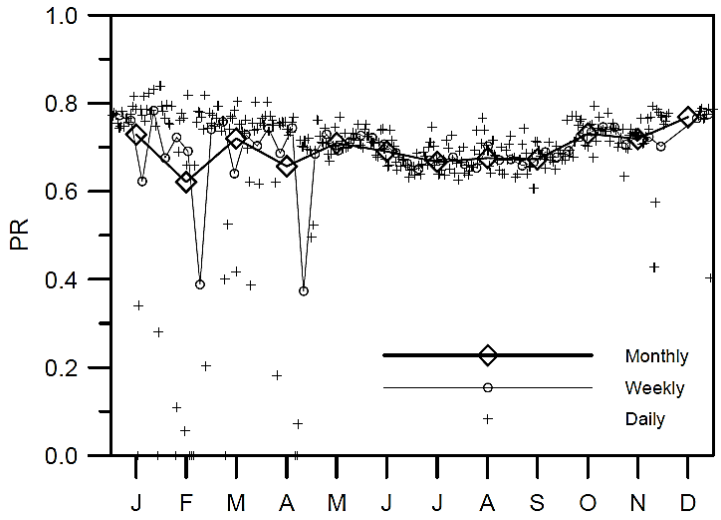

Figure 2.2 Daily, Weekly, and Monthly PR Values for the PV System in 2001[62] [60].

However, the significantly reduced PR represents faults/anomalies in the PV system, such as partial shadings, inappropriate system sizing, MPPT errors, inverter failures, and faults within PV arrays. In addition, Fig. 2.3 shows that P_r values for smaller intervals (such as daily) give better fault-detection resolution and quicker response than monthly or weekly data [63].

2.1.2 Machine Learning based Methods

Machine learning is a subarea of artificial intelligence, which automatically extracts knowledge from the given PV data set. One category of the machine learning uses supervised learning approaches. As shown in Fig. 2.4, depending on a large amount of labeled data, supervised learning algorithms can learn the system and make the prediction after it is trained. A variety of supervised learning models have been proposed in PV installations. Artificial Neural Networks (ANN) is developed for PV performance evaluation under partial shadings [64], PV health status monitoring [65] and short-circuit fault detection in PV arrays [66]. Bayesian Neural Network (BNN) and regression polynomial models have been proposed to predict the soiling effects on large-scale PV arrays [67]. PV fault detection and classification use decision-tree model in [68], K-nearest neighbor and support vector machine (SVM) in [69].

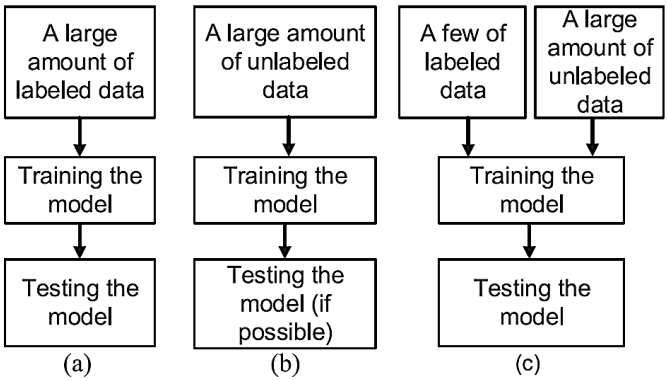

Figure 2.3 Simplified Flowchart of Machine Learning Techniques.

(a) Supervised (b) Unsupervised learning (c) Semi-supervised learning.

In the case of given knowledge surrounding faults it is possible to apply supervised learning, e.g. [68], where a labelled dataset is available containing

measurements classified manually. This dataset can for example be generated by measuring voltage and current of solar modules while injecting faults. The paper discusses a decision tree model that takes the available measurements and locates the most probable classification based on the dataset. Classification performance is concluded to be very good but real-life applications are limited due to the dataset being heavily tied to a specific PV installation. A natural extension is analyzed in [70] which considers the case of graph-based semi-supervised learning, where only a small amount of reference data is available from the start as in Fig 2.4. This approach results in significant cost reductions, due to the low amount of labeled data, but is also possible to adapt to changing conditions in different systems. The classification performance is up to 99% for certain classes of errors.

2.1.3 Statistical Methods

Statistical methods are proposed to detect abnormality in PV systems based on energy generation [71]. Specifically, descriptive and inferential statistics are applied on the measured energy generation of each subarray of a PV plant. The experimental results show that the proposed method can successfully detect a wiring mistake at a single PV panel out of 22 normal panels. Multivariate outlier rules using minimum covariance determinant (MCD) has been proposed for PV fault detection [72]. Specifically, based on a number of voltage and current measurements of PV modules at each specific time, the MCD is used to calculate the robust distance (RD). The fault detection rule becomes straightforward: if the calculated RD is larger than a threshold, the fault occurs in the PV module. Another statistical approach is taken by Zhao [73] that is centered on outlier

detection. Similarly, to [54, 55], the paper assumes a set of identical PV strings and tries to classify deviations. This is done by building confidence intervals using three different methods: 3-Sigma rule, Hampel identifier, and Boxplot rule. All the surveyed methods exhibit different properties, but the paper concludes that the Hampel identifier and Boxplot rule are suitable for fault detection. Based on the assumptions made, the paper can consider all PV string currents as samples taken from a single normal distribution, allowing straight-forward statistical analysis. This simplification is however not applicable in practical real life situations.

Finally, [74] takes the approach of using a Kalman filter in order to predict power output. The Kalman filter [74] takes a set of noisy measurements and the underlying physical model, and produces the most probable output value in an iterative process. This is used in order to locate faults based on measurements of voltage, current, and panel temperature. Notably this permits classification without access to irradiance data. However, access to panel temperature is required for this method. There has also been research into locating the faulty panel within a string [75]. These results can be considered less applicable when individual solar module measurements are available.

2.2 Topology Optimization Methods

The Figure 2.5 shows a block diagram that summarizes the vision for optimizing a utility scale PV array. The monitoring devices connected to every PV module collect the individual module measurements (current, voltage and temperature) continuously. The collected information is transmitted to the server which stores past and current measurements of panel and weather data. A central operator accesses the data and can

take action and issue various control commands to the PV array and the inverters. The output of fault detection algorithm is used to determine PV array topologies that optimize the overall efficiency of the array for different environmental conditions. This section focuses on the 'Connection topology reconfiguration' block, which is equipped with reconfiguration algorithms to predict the optimal array topology. There is a need for dynamic reconfiguration of the PV array topology to ensure effective power generation under any shade condition.

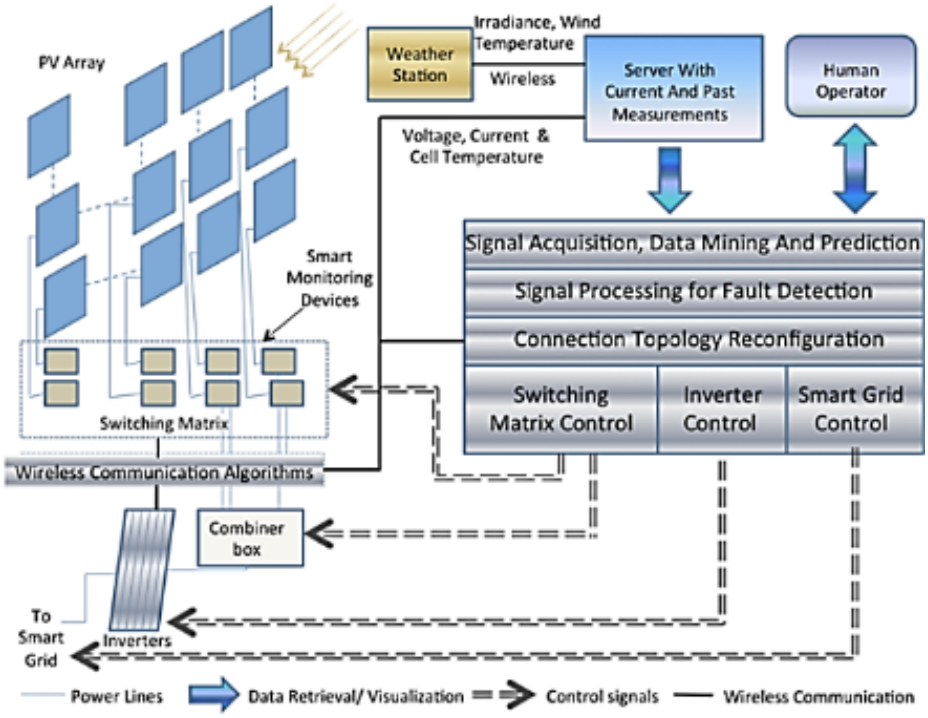

Figure 2.4 Intelligent Networked PV System Management [76, 92].

The major problems that cause the PV array to generate power less than the rated power are shading and improper selection of topology. To overcome the shading problem, several methods were put forward. The leading-edge research area which is developing called dynamic reconfiguration strategies, namely efficient ways to

dynamically change the connection layout of PV modules into PV arrays in order to improve power output under electrical mismatch conditions caused by partial shading and other issues. For instance, when one or more series-connected PV modules are shaded, the maximum permitted current is reduced, consequently decreasing the power output [77]. Moreover, the shaded or faulty module can reach critical high temperature, leading to the hotspot phenomenon [78–82] and consequently to the failure of the module. Bypass diodes avoid the hotspot and mismatch events [83, 84], but they introduce losses and local maxima in the electrical characteristics of the PV module [85].

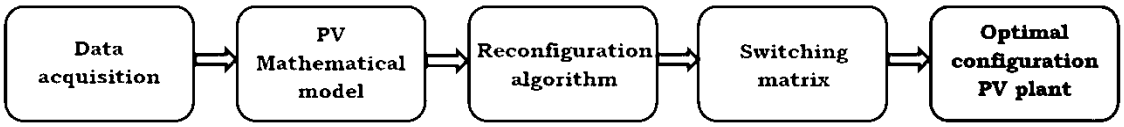

Figure 2.5 Block Diagram of Topology Reconfiguration Block.

Electrical Mismatch and Partial Shading

Differences in electric characteristics of solar cells lead to mismatch losses [86, 87] inside the module, while modules with different electrical characteristics lead to mismatch in the whole PV plant [88]. Both issues can be influenced by factors that are internal or external to the module. Internal factors include non-homogeneous characteristics of solar cells, caused by manufacturing defects, faulty solar cells and malfunction of one PV module [68]. External factors include degradation of materials used to encapsulate the cells, dirt deposited on the cell surface, different temperatures [89] and shading [90]. In particular, partial shading of PV modules occurs when these are subjected to passing clouds, smog layer or common urban elements such as chimneys, electricity pylons and surrounding buildings and dirt. When modules with different

electrical characteristics are connected in a PV array [91], the mismatch issues become critical. In fact, the solar module in the worst operating condition determines the output current of the entire series-connection, leading also to non-recoverable reverse bias breakdown, hotspot phenomena and excessive power depletion as a result of mismatch effects [78] [91–93]. Since mitigation of mismatch losses in a solar array is always necessary, most commercial PV modules incorporate one or more bypass diodes, inserted in parallel to a group of cells series- connected [95].

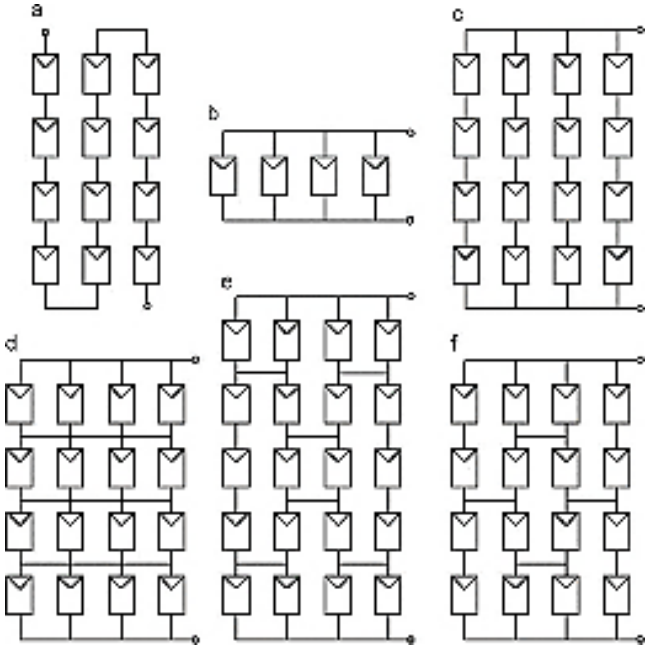

Figure 2.6 Connection Topologies of the PV Array.

(a) Series array, (b) parallel array, (c) series-parallel array, (d) total-cross tied array, (e) bridge-link array and (f) honey-comb array.

The presence of bypass diodes significantly affects the electrical curves of the PV array and creates one or more local maximum power points (MPP) in the P–V characteristic when a significant mismatch occurs, see Fig. 2.1. Therefore, distortion of

shaded I–V curve may lead to an error in the determination of the global MPP [93]. In the literature, some efficient simulation tools have been described [96–98].

2.2.1 Reconfiguration Strategies

In the literature, many alternative array interconnection topologies have been proposed for reducing mismatch losses [99–100]. Series and parallel topologies, Fig. 2.7 a and b, are the basic configurations, with the main disadvantages that, respectively, the current and the voltage are below the practical desired values. During partial shading, parallel-connected PV elements produce higher power than series-connected ones, since in the parallel connection the overall current is the summation of all the currents [81] and voltages do not vary very significantly [101]. However, higher currents flow in parallel-connected elements, so that power losses [102] and voltage drops are generally higher and cabling is more expensive. In actual PV power plants, the serial-parallel (SP) is the most common connection. It is obtained connecting solar modules in series to form a string (necessary to reach the voltage required by inverter input ranges); strings are then connected in parallel to increase the total current (as shown in Fig. 2.7).

In Total cross-tied (TCT) configurations (see Fig. 2.7 d), modules are first parallel tied so that voltages are equal and currents are summed up; many of these groups are then connected in series. Though under uniform conditions SP and TCT modules connection provide the same power value, the TCT topology reduces the overall effect of mismatch. In the Bridge-link (BL) topology, in Fig. 2.7 e, about half of the interconnections of the TCT topology are avoided, so that cable losses and wiring installation time are reduced [103]. Though, in larger installations the TCT arrangement can be easier to wire because

of the simplicity of the pattern [99]. Advantages shown by both TCT and BL topologies have been combined in the Honey Comb (HC) configuration (in Fig. 2.7 f). Although many convenient interconnection topologies have been developed, so far the most exploited solutions rely on TCT and SP module interconnections. In the following sections, the different reconfiguration approaches proposed in the literature have been discussed.

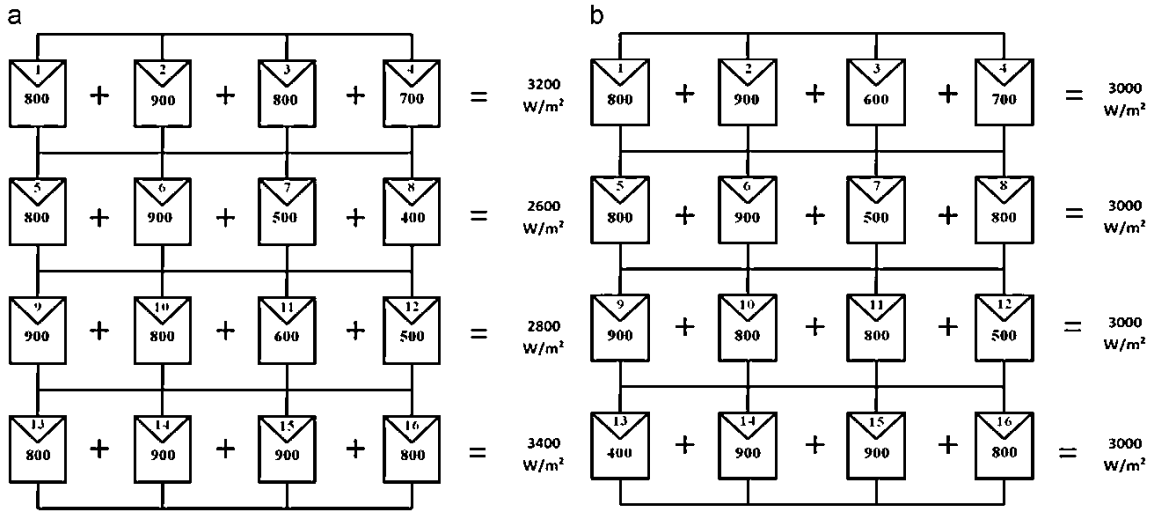

Figure 2.7 Irradiance Equalization Example.

(a) Before sorting, rows have different irradiance levels: 3200, 2600, 2800 and 3400 W/m2; (b) changing PV modules position following a reconfiguration approach (modules 3–11 and 8–13 have been switched, the irradiance could be equalized as 3000 W/m2) [104]

2.2.2 Reconfiguration for TCT Topology

As already discussed, the TCT interconnection allows to reduce the overall effects of mismatch. The challenge in a TCT reconfiguration technique consists in connecting

PV modules in irradiance-balanced tiers. An interesting optimization algorithm based on the use of an equalization index was presented in [104]. Irradiance equalization aims to obtain series connected tiers, also called rows, where the sum of the irradiances of the modules is the same; this results in a string where the circulating current is proportional to the given sum of irradiances of one row.

The algorithm equalizes the available power on each row, thus n ideal current generators, with the same nominal values, are connected in the string, avoiding mismatch losses. Indicating with G the irradiance value of the module located on row I and column j within the topology showed in Fig. 2.8, the total irradiance of the row i is defined as

$$G_i = \frac{\sum_{j=1}^{m} G_{ij}}{m} \tag{4}$$

where m is the number of modules that are parallel connected. For each configuration, the algorithm calculates the equalization index (EI) by means of the following expression:

$$EI = \max_i(G_i) - \min_i(G_i) \ \forall \ i \tag{5}$$

This index quantifies the degree of current limitation of the configuration and thus the one minimizing EI is selected. The secondary aim pursued by the algorithm is the smallest number of switching operations starting from the initial configuration. Under the same equalization index, the configuration with the least number of switching operations to be performed is selected. In [105] a PV generator with an electrical array configuration (EAR) controlled by the irradiance equalization algorithm has been presented. The EAR PV generator is composed of a static part, necessary to meet the input range constraints of the inverter and are configurable one, controlled by the irradiance equalization algorithm.

Although all the possible interconnections of PV modules are (m.n)! the total configurations of interest (C), namely the configurations delivering different values of output power, are

$$C = \frac{(m.n)!}{m!.(n!)^n} \tag{6}$$

with m and n, the number of rows and columns. All the configurations of interest can be achieved by using a number of switches, N_{SW} equal to

$$N_{SW} = 2N_{PV} \tag{7}$$

These N_{SW} switches are of single-pole m-throws type and N_{PV} is the number of PV modules. It should be noted that, if not commercially available, it is necessary to emulate a m-throw switch by connecting m single pole switches in parallel, thus increasing N_{SW} by a m factor as well as the overall control complexity.

A variation of this technique was proposed in [106] as a mixed integer quadratic programming problem, which can be also applied when a non-equal number of modules per row is considered. In [107] a particular switching matrix, named Dynamic Electrical Scheme (DES) is proposed. It allows to implement two different reconfigurable controlling algorithms by computing the irradiance equalization. This solution creates rows with a non-equal number of modules, thus increasing the number of possible interconnection configurations. Calculation time, for a given number of modules, is fixed for the deterministic search algorithm, while in the random search algorithm it depends on the ending condition (e.g. prefixed number of iterations or flattening criterion). By the deterministic search algorithm, modules are ordered within the topology according to

decreasing irradiance values. First, the minimum ($N_{row\ min}$) and maximum (N) number of rows of the optimized PV array are set. The algorithm then looks for the optimal configuration starting with a number of rows (N_{row} max) equal to $N_{row\ min}$. The first N Rows modules of the decreasing sequence are located one per row; then the remaining modules of the sequence are one by one connected to the row for which the sum of the irradiances of the modules already positioned is the minimum. After the last iteration, all modules are located and the total irradiations of rows are known. Then the algorithm calculates the equalization index by means of EI equation and stores it. The number N is thus increased and the same procedure is repeated until N. Finally, the optimal configuration is the one that minimizes the equalization index.

The DES requires a number of switches N_{SW} equal to

$$N_{SW} = (2mN_{PV})_{DPST} + (m)_{SPDT} \quad (8)$$

where DPST are double-pole single-throw switches, N_{PV} is the number of PV modules and m is the number of rows, supporting up to (m n)!/(n!)^m configurations. Another method based on the irradiance equalization principle was presented in [108]. The proposed technique is an iterative and hierarchical sorting algorithm, designed to achieve a near optimum configuration in an efficient way in terms of number of iterations. The irradiances of cells are obtained, arranged in descending order and mapped to the matrix of the physical PV array. Next, all even rows are flipped left to right and added to the preceding odd row, resulting in an averaged matrix. This method is applied again, resulting in a second average. The process stops when all the rows have been considered. A number of padding rows of zeros can be added if the number of rows is not a power of

two nor an even number. Although the proposed interconnection matrix supports each row having arbitrary number of modules, the algorithm enables to build rows having the same number of modules only. If single-pole single throw (SPST) switches are used, the number of required switches, N_{SW} is

$$N_{SW} = N_{PV}.(m^2 - m) \tag{9}$$

where m is the number of rows. In [109], a system architecture enabling the adaptive interconnection of solar cells inside a PV module was presented. This solution can be extended to a PV plant, where, instead of solar cells, many modules are considered. In this approach, a switching matrix connects a fixed number of fixed PV cells in a TCT topology, to another small reconfigurable (not fixed) bank of solar cells [110]. The number of switches required by this approach is smaller when compared to other solutions, for the presence of affixed part, thus enabling the use of simpler controlling algorithms. Under uniform irradiance conditions, static part and the adaptive one are connected together through the switching matrix. If the first row is shaded, its voltage V_1 is less than a threshold voltage; otherwise, when the j^{th} row (with $j \neq 1$) is shaded, the output voltage is less than the quantity V_X

$$V_{out} < V_x (where\ V_x = mV_1) \tag{10}$$

where m is the number of rows. Both conditions trigger the reconfiguration phase. The logic of this approach relies on connecting the most irradiated cell of the bank (with the maximum open-circuit voltage) to the most shaded row of the fixed part, in order to compensate the irradiance (and thus the voltage) drop.

A simple bubble-sort method and a quick model-based method are presented in [111] for controlling the switching matrix. In [112] a self-adaptive reconfiguration method based on fuzzy logic was proposed. When the voltage across a row is less than the threshold, the shading degree and the derivative of the irradiance are calculated, and then used as the inputs of a fuzzy controller. The latter calculates the number of PV cells of an adaptive bank needed to compensate the irradiance drop and then the reconfiguration is carried out. Finally, in [113] the Su Do Ku puzzle pattern is used to physical arrange modules in a TCT connected PV array, distributing the shading effects over the array and consequently reducing the occurrence of shaded modules in the same row.

2.2.3 Reconfiguration in SP Topology

Reconfiguration by means of SP topology aims to build strings of series-connected modules with similar irradiance levels and then connecting all these strings in parallel. In this way, well irradiated solar panels will not be limited in current by a low irradiance panel of the same string.

A Flexible Switch Array Matrix (FSM) was presented in [114]. The FSM is integrated with PV modules to form the Elastic Photovoltaic Structure (EPVS). In uniform conditions, the PV system operates as a central inverter topology and the DC/DC converter is not used. When mismatch occurs, the proposed system excludes the shaded PV modules, reconfiguring the remaining ones in the main PV strings (MPV) and, if necessary, a sub-PV string (SPV). MPV strings have an equal number of modules connected directly to the inverter input, while SPV has fewer modules so that the DC/DC

converter is used to connect this partial string to the inverter, thus avoiding mismatch losses. Four single-pole dual-throw (SPDT) switches are needed for every module, while two are required for the MPV bus and other two more for the SPV. The total number of required switches, N_{SW} is given by the expression:

$$N_{SW} = (2N_{PV})_{SPDT} + (2N_{PV} + 4)_{SPST} \quad (11)$$

where N_{PV} is the number of modules and 4 are the switches required for the MPV and SPV bus. The identification of the irradiance conditions of PV modules was achieved by measuring voltage, current and temperature of each module. In [115] a 9 module prototype system implementing this approach is presented, showing power gains compatible with simulation results.

Another approach using DC/DC converter is presented in [116], where multiple strings, each containing substrings of similar power levels only, were created. All the strings were connected to a DC/DC converter array, converging to a unique dc bus. In [117] the aim was to build strings where solar cells having similar irradiance levels, G, are connected. First, the current (I_b) across every bypass diode of each cell is sensed; when I_b is greater than zero the cell is dark, otherwise the short-circuit current (I_{SC}) is measured to classify the cell as bright or grey. The proposed strategy calculates the number of shaded (dark) cells and if this is greater than 15% of the total, the reconfiguration occurs. Cells of the same state are combined in strings (bright strings and grey strings), while dark cells are excluded from the array, since their power contribution is negligible. The proposed system senses temperature and open-circuit voltage of each cell for monitoring purposes [118].

In [119] the Rough Set Theory (RST) is used to build an Automatic Reconfiguration System (ARS). For a SP topology of PV modules, different cases of shadowing conditions (when one or two modules are shaded) are considered and, for each of them, the most convenient SP connection of PV modules is selected. The RST helps to recognize similar or equivalent cases, producing simplified rules starting from the data of a decision table [120]. Each module of the PV array supplies a certain value of current i(k). When i(k) is less than a threshold current I_{ref} (i(k) I_0), the module is considered 'shaded'; on the contrary, if i(k) 4I the module is considered 'unshaded'. For every module of the PV array, the information about its shading state is used by the set of rules and the correct rule is chosen. Every rule contains a switch configuration which sets the optimal configuration for the electrical connections of the panel.

To summarize, some of the most interesting PV reconfiguration strategies for different PV plant topologies presented in the literature have been discussed. While many commercial solutions rely on the classic Series Parallel topology, the Total Cross Tied topology has raised a great interest from many authors. TCT offers effective optimization algorithms and higher flexibility, despite the higher currents of this topology usually lead to more expensive cabling, thus reducing the Return-on Investments (ROI) index. Furthermore, for small PV plants the overall voltage plant output is less than in the case of the SP topology. On the other hand, marketing target in the next years, could be the conversion of fixed PV plants into reconfigurable ones; in this way, keeping the SP topology will save re-designing efforts and costs. Adding a dynamic reconfiguration system to an existing PV plant that benefits from a particular feed in tariff would produce not only an increase of the energy produced but also an increase of the economic

advantages connected to the relevant feed in tariff. Nonetheless, it could be possible to design a reconfigurable interconnection device supporting both SP and TCT interconnection topologies at the same time, but on the other hand, many switches would be needed and, as a result, costs would be increased. Therefore, the interconnection topology should be chosen first. While it could be possible to address the TCT connection topology for new plant designs and the SP for the conversion of existing plants, a better comparison study on the TCT versus SP reconfigurable approach should be needed in terms of investments, reliability and power improvements. The overall complexity of the solution and total cost are indeed important factors to evaluate a proper reconfigurable approach. Further research on the topic should be addressed towards the definition of efficient switching matrices also taking into account the lifetime of switches, not only installation costs, as well as the identification of applicability issues for each considered strategy.

2.3 Solar Monitoring Methods

A monitoring system for a PV array is usually needed to collect power production and performance data as well as weather conditions. Several systems have already been developed to monitor PV arrays and modules. We look into some of these systems currently being used emphasizing systems that perform intra-array monitoring. The usability of each system varies depending on their targeted capabilities. This data enables to track the working conditions of each module, recognizing faulty solar panels, mismatch and partial shading conditions [121–124]. Monitored variables of interest are DC and AC electrical parameters (voltage, current, power), module and ambient

temperature, irradiance, wind speed and humidity [125,126]. While the majority of monitoring systems collect data at a whole plant level, sensing parameters that are closer to each module are necessary when a PV module fault detection and reconfiguration approach is adopted. As detailed in Section 2.2, most open loop control systems employed for dynamic reconfiguration purposes use the irradiance value since the irradiance equalization algorithm [127] requires the knowledge of the irradiance for every PV module. The most common method to sense the irradiance employs a pyranometer, thus common solar plants have one or few units for monitoring purpose. In order to have a good understanding of the spatial irradiance profile, one pyranometer per PV module should be used, consequently increasing costs. In chapter 4, approach estimates the irradiance level of each solar module by measuring the electrical characteristics of the modules. Voltage, current and temperature can be used in combination with the physical parameters of the given solar module to obtain the irradiance value using the PV electrical model in one diode model. In [104] and [114] a simplified model was used to estimate the irradiance, starting from the voltage and the current of the module. However, in many real-world situations, temperature effects should not be neglected since, under shadow conditions, the temperature difference between modules can be significantly greater than zero. Thus, the irradiance levels can be considerably different even if modules have compatible values of voltage and current.

It is worth mentioning that, while in a SP topology it is necessary to acquire the voltage for each module but only the current of each string, in a TCT topology the voltage of every row and the current of each module are needed. Thus in a TCT topology more current sensors are used. Another approach relies on short circuit current sensing of

each module, estimating irradiance. The advantage of this method is that ISC has a linear dependence on irradiance [128] and also is not very sensitive to temperature variations, thus temperature measurements are not necessary. This approach however requires each solar module to be electrically disconnected from the PV array and to be short-circuited for every measurement, not only causing lack of its power contribution, but even leading to the stop of the inverter MPPT algorithm if the minimum voltage and current input ranges are not satisfied due to its exclusion. In order to avoid installing current sensors, usually more expensive than voltage sensors, the open-circuit voltage V_{OC}, I_{SC} and the temperature of each module can be measured and estimating irradiance. Even in this case, each solar module will be electrically disconnected from the PV array. In [128] a similar approach was used to evaluate irradiance levels, although the temperature is not acquired for each module. Monitoring a fixed PV plant in order to evaluate the affordability of its conversion to a reconfigurable plant is an issue of great interest. For such application, a wireless monitoring system [129] could be adopted for sensing the electrical characteristics of each module of the plant, thus processing the acquired data to evaluate the power improvement that could be obtained using a reconfigurable interconnection matrix.

A monitoring system used to evaluate the performance of PV array installed on a building is given in [130]. The monitoring system measures voltage, current and power at the AC output of the inverter. It measures the solar intensity using two photo diode sensors and taking their average. Module internal temperatures are obtained using temperature sensors. The measurements are done over 20 minute intervals. The data can be used for both short term purposes such as monitoring the system's status, and long

term purposes such as monitoring the deterioration of components. Comparison of the different strings helps evaluate the effect of shading on the array. The correlation of output power with temperature can be used to determine the effect of module temperature on output power for the same irradiance. These measurements can be used to evaluate the annual energy production and cost of electricity produced by the array. Measurements are transferred to a computer enabling internet access to the data. The authors mention the use of commercially available data acquisition systems to transfer the data to the computer. Here, the monitoring system does not consider module level measurements and communication systems for such an arrangement. Kolodenny et.al [131] propose an approach that uses modern informatics tools such as XML to analyze the acquired data. Their goal is to analyze the performance of a PV system of any type and size. They propose a protocol called PV markup language (developed from XML) to automatically access, extract and use data from several sensors systems/database sources. The system collects and classifies the data.

A PV logger system constantly collects information about the state of the array (such as voltages, currents and irradiance) and updates it in a database. The system diagnostics retrieves the data and detects possible failures. This information is then updated in the database. The different users can query the database and obtain information they are interested in. The owner can view the overall system health and output of the array while the technician can view the PV system parameters. This work provides a comprehensive method to store and retrieve PV array data and can be used with different current voltage sensor location and weather data. However, it does not describe a complete PV monitoring system which includes sensing, data communication and user interface

systems. A simple and cost effective method of monitoring a PV power station using a GUI built in NI LabVIEW is presented in [132]. The set-up consists of current sensors for each string and voltage sensor for the array connected to a micro-controller through an analog multiplexer. Irradiance is measured using a pyranometer. Also included are sensors for measuring the module surface temperature. The collected data can be used for both monitoring and control. The micro-controller is interfaced to a laptop through a serial port where the data can be viewed and analyzed using a GUI designed using LabVIEW. The GUI provides views for PV array output and battery health and calculates PV expected outputs using the diode equivalent model given in Figure 1.2. This system does not consider module level sensor networks and communication systems for them.

Chapter 3

PV ARRAY MONITORING SIMULATOR

3.1 Overview of System

This section provides a brief overview of the smart PV array monitoring simulator developed in laboratory environments. The simulator attempts to represent a PV array with a large number of PV modules, each attached to a smart sensor device as shown in Figure 3.1. These smart sensors communicate through a wireless sensor network with a monitoring station from which data and analytics can be obtained using an Internet connected smartphone, tablet or desktop PC.

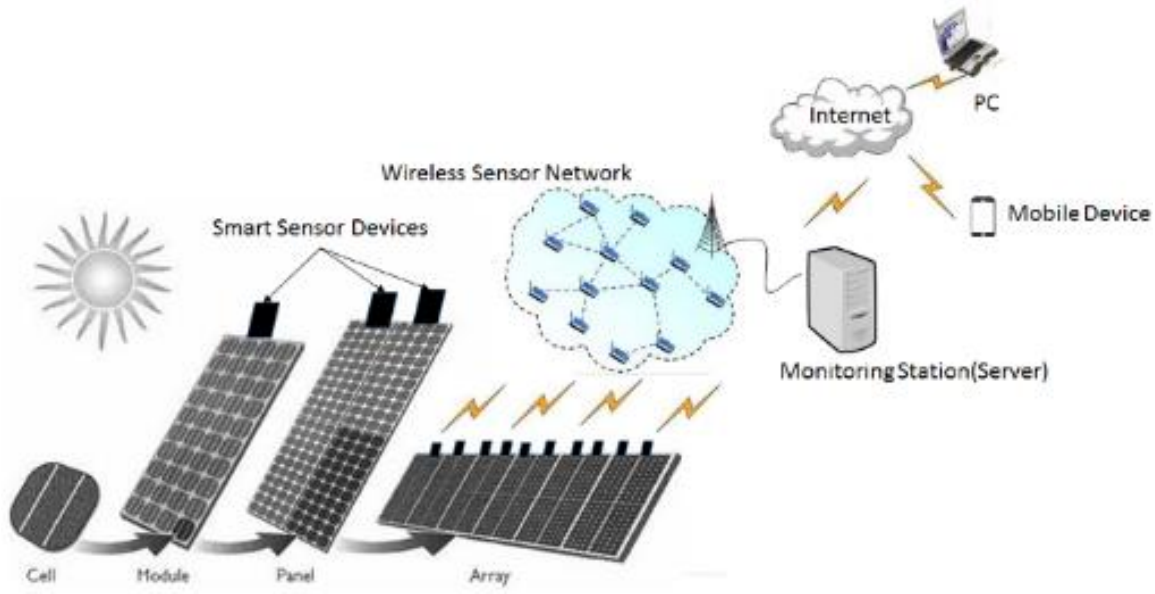

Figure 3.1 Concept of Smart PV Monitoring System.

For the small scale simulator implementation, this monitoring system can be divided into basic building blocks as shown in Figure 3.2. The PV array laboratory simulator consists of a 4x4 array of solar panels in which 4 modules are connected in a

series string, and each of these 4 strings are then connected in parallel. In actual field applications, monitoring is required for hundreds or thousands of panels. For the lab monitoring simulators, voltage dividers are used as voltage sensors.

Other sensors include current sensors [133] based on variable resistors to detect current in each series string, a light-to-frequency meter to detect irradiance, and digital temperature sensor [134] for temperature.

In our simulator, these sensors are connected to a 10-bit ADC of the ATMEGA328 microcontroller (part of Arduino Uno), which converts the analog signal to digital. The board is connected to the PC running LABVIEW and LABVIEW Web Services. The last sub-block is the end user, who can access data through a webpage or an app.

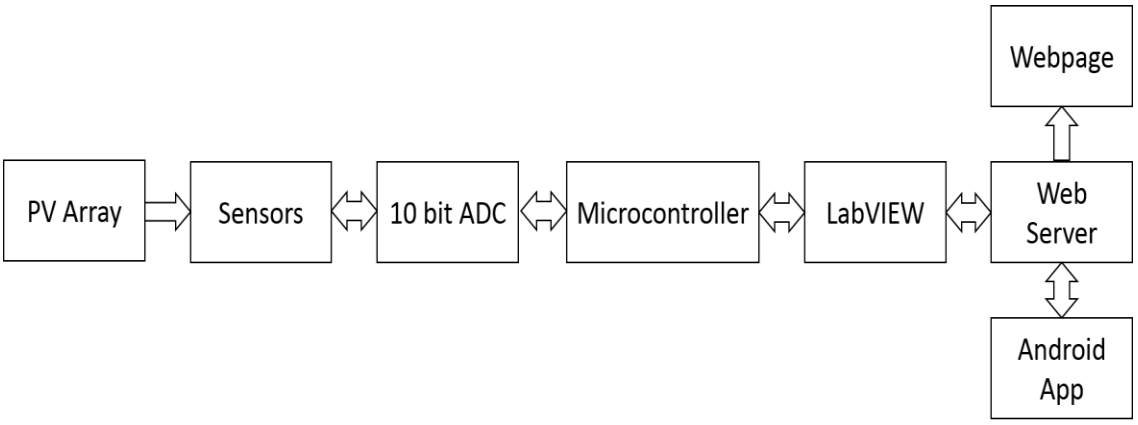

Figure 3.2 Block Diagram of the Implementation.

The implementation of the compact monitoring simulation system involves hardware and software design which will be discussed in the next sections. The data flow and the components involved is shown in Figure 3.3.

3.2 Hardware and Software Setup

Hardware Design

The hardware design includes two sections. The first is the PV array setup which describes the array configuration, sensors connected to array, and its topology connections in detail.

The next section is the measurement circuit which discusses the sensors connected to this circuit, capability of Arduino board and its shields, as well as data communication of sensors to the measurement circuit and serial communication of the measurement circuit to PC.

PV Array Setup

Table 3.1

Solar Panel Parameters.

Symbol	**Cell Parameters**	**Typical Ratings**	**Units**
V_{OC}	Open circuit voltage	5.04	V
I_{SC}	Short Circuit Current	200	mA
V_{MPP}	Voltage at MPP	4.00	V
I_{MPP}	Current at MPP	178	mA
P_{MPP}	Max. Peak Power	714	mW
FF	Fill Factor	>70	%
η	Solar cell efficiency	22	%

The PV array consists of 16 solar panels (Part No. SLMD481H08L from IXYS Corporation) [135] in series-parallel configuration. PV panel parameters are given in Table 3.1. First, four solar panels are connected in a series string; each of these four strings are then connected in parallel to create a 4x4 array as described in Section 3.1.

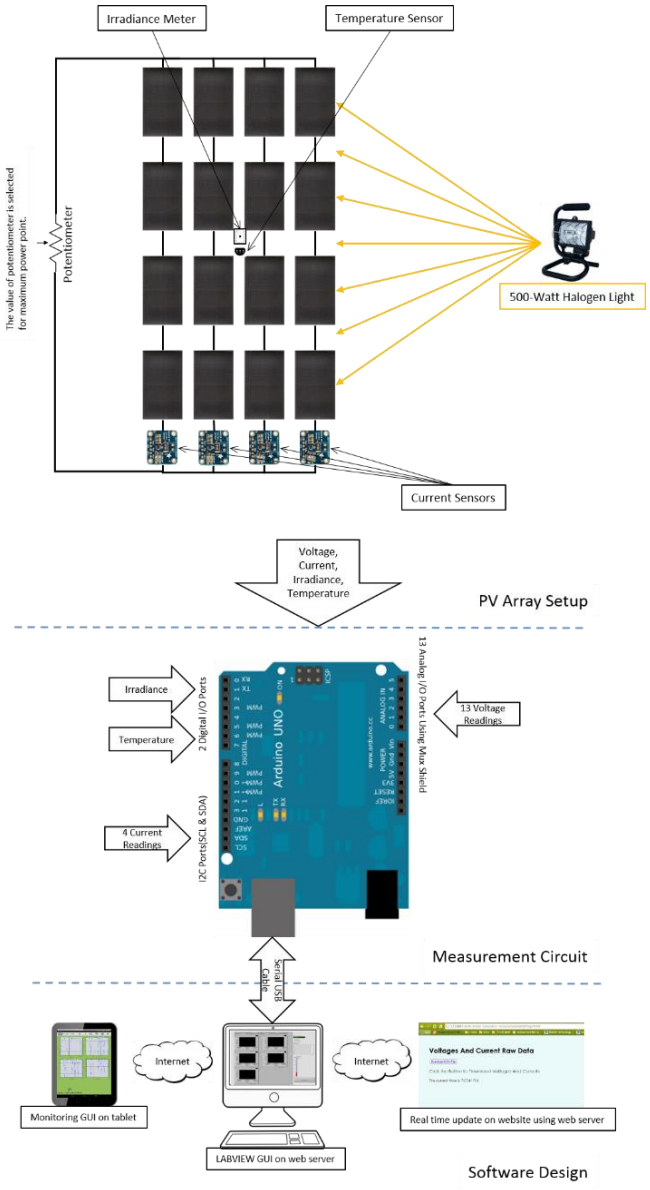

Figure 3.3 Solar Array Monitoring Simulator: Implementation Architecture and Data Flow.

The nodes in-between each of the solar panels are also connected to multiple voltage divider circuits acting as voltage sensors as shown in Figure 3.4. The 13 single-ended voltages with respect to ground are fed to the measurement circuit, which computes the individual solar panel voltages. The measurement circuit has analog voltage input capacity of 0V-5V. The resistors in the voltage divider circuit are chosen in the ratio of 4:1 so that the maximum solar panel series string voltage (i.e. 20V) can be handled by the measurement circuit. A 1nF capacitor is also connected across the voltage divider to filter fluctuations in the analog voltages.

Four current sensors (INA219) are used in series with each of the four series strings of solar panels. These current sensors are based on the principle of variable sense resistors and can measure up to 3.2A with a precision of 1%. Current readings from these current sensors are communicated to the measurement circuit using I2C. The temperature sensor (DS18B20) is a digital temperature sensor, and is connected to a digital port of the measurement circuit through a 4.7kΩ pull-up resistor. This temperature sensor has precision of 0.5°C. The TSL230BR−LF programmable light-to-frequency converter [136] is used as an irradiance sensor. This combines a configurable silicon photodiode and a current-to-frequency converter on single CMOS IC. The photodiode's working wavelength range is from 320nm to 1050nm. Sensor output is a pulse train with frequency directly proportional to the irradiance on the photodiode. Pulse train output is connected to one of the PWM ports of the Arduino board. To complete the PV setup, a 500W halogen lamp is used for the light source in the lab environment. The PV array is connected to a variable load (potentiometer) to plot voltage-current (V-I) and power-voltage (P-V) characteristics curves.

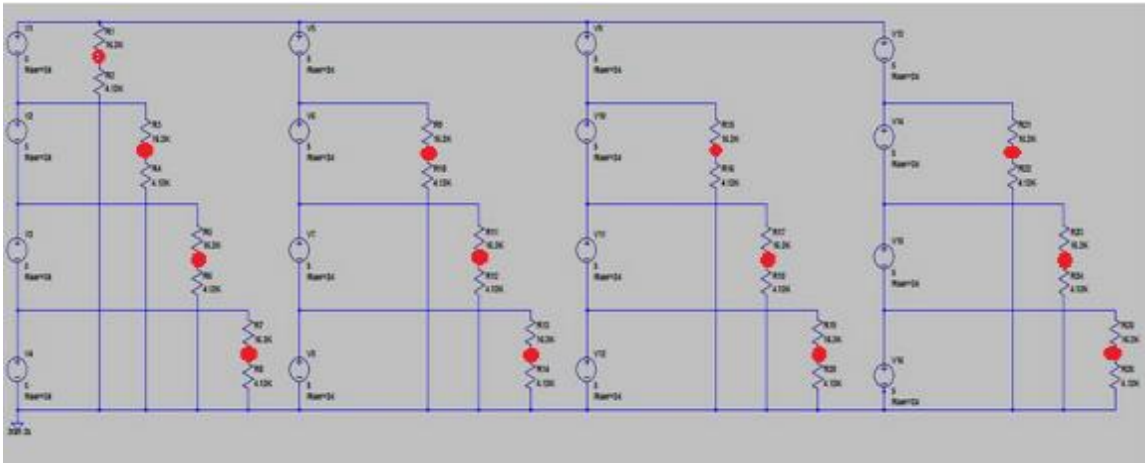

Figure 3.4 Voltage Sensor Circuit with PV Array.

Measurement Circuit

The heart of the measurement circuit is the Arduino Uno board which communicates with a PC as well as multiple sensors in the PV array setup.

Table 3.2

Communication Ports of Measurement Circuit.

Symbol	**Communication Protocols**	**Arduino Ports**	**Number of ports**
Voltage	None (Analog Voltages)	Analog I/O	13
Current	I2C	SCL & SDA	2
Temperature	1-Wire Protocol	Digital I/O	1
Irradiance	PWM	Digital I/O	1

It is a microcontroller board based on the ATmega328 microcontroller. The Arduino has 14 digital input/output pins (of which 6 can be used as PWM outputs), 6

analog inputs, and a 16 MHz ceramic resonator for clock. A multiplexer shield is connected over the Arduino board to extend its capacity from 6 to 48 analog I/O ports.

The communications channels and protocols for all the sensors have been listed in Table 3.2. The USB cable connected from the Arduino to the PC provides power for the sensors and a UART serial communication channel for transmission of sensor data. Then, using LABVIEW on the local PC, web server data can be displayed on a PC or mobile device.

Software Design

Software design was completed in multiple phases, including Arduino IDE programming, LABVIEW programming, HTML programming and smartphone app programming. We describe the details in the following.

Arduino IDE Programming

Arduino can be programmed using Arduino IDE in what is called a sketch. The sketch contains code to run a mux shield, temperature sensor, current sensor, irradiance sensor, etc. by using multiple support libraries for each sensor. A snapshot of the sketch using Arduino IDE is shown in Figure 3.5. The communication link is established when Arduino board is connected to the local PC running LABVIEW before transmission of data.

The Arduino board communicates with the PC using a serial connection with Baud rate 115200 bits/s. The first data packet transmitted is the temperature reading. After constant intervals of time voltage, current, and irradiance readings are transmitted.

The next packets of data consist of 16 computed voltage readings, 4 current readings and 1 irradiance reading.

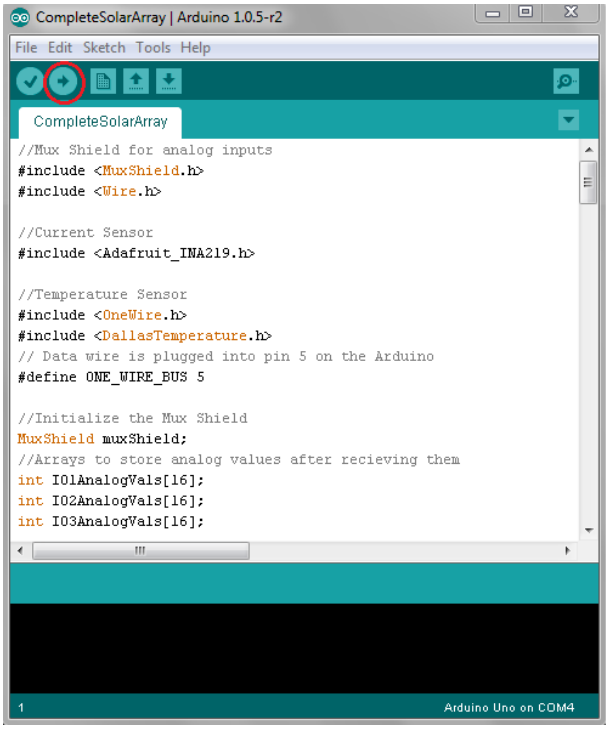

Figure 3.5 Arduino Sketch in Arduino IDE.

LABVIEW Programming

The LABVIEW project includes programs related to communication with Arduino, a display GUI for use on the local PC, and a web service for remote viewing of system data. Once the communication link is established between Arduino and PC, the character data is converted to numeric data, which is then displayed on the LABVIEW GUI as shown in the Figure 3.6. The PC GUI is divided into 5 tabs. The first 4 tabs each display the current through one string and the voltages of the 4 modules within that string. The final tab displays a scatter plot of the V-I operating points and the I-V and P-V characteristics of the array.

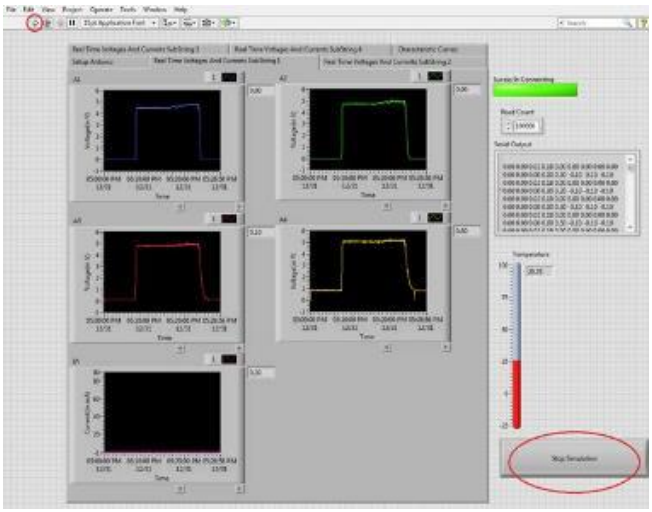

Figure 3.6 LABVIEW GUI Displaying Voltages, Current, Temperature and Irradiance.

At the right side of the GUI, temperature and irradiance are displayed. The block diagram of the LABVIEW program (Figure 3.7) also shows connections between different LABVIEW blocks to run the LABVIEW web server.

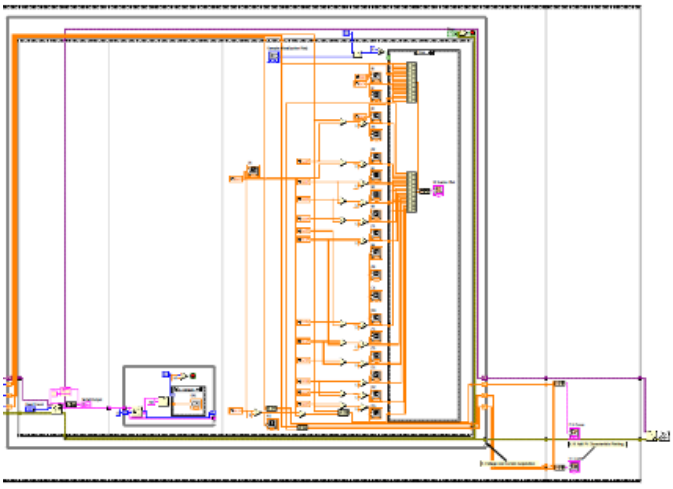

Figure 3.7 Block Diagram of LABVIEW Program.

Measurements are logged in .csv files at all times. The LABVIEW block diagram also makes data variables available to an app that is running on a smartphone or tablet.

Webpage and Smartphone App Programming

The LABVIEW web server has a webpage running on it which displays a description of the project and the data from the PV array setup. Using this webpage, sensor data stored in .csv files can be accessed remotely and analyzed with ease. Previously stored data for multiple operating conditions is also available as sample data when the web server is offline. The app required to display data remotely is Data Dashboard for LABVIEW (available on major mobile platforms). The app's GUI display is similar to the PC GUI, but with additional optimizations for widely varying screen sizes of smartphones and data is sampled at every 0.3s. Larger screens devices like tablets automatically display more data than a smaller screen device like a smartphone.

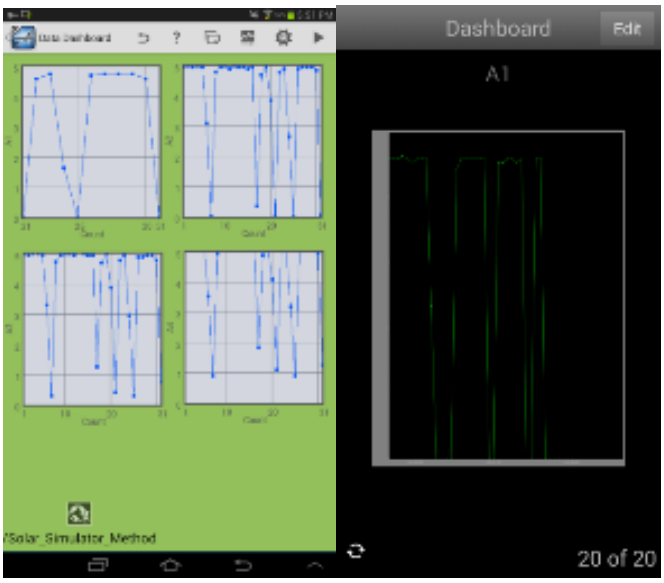

Figure 3.8 App Running on Tablet and Smart Phone.

Figure 3.8 shows a snapshot of the app displaying four analog voltages of series connected solar panels (A1-A4) on a tablet and another snapshot of the app displaying analog voltage of single solar panel (A1) on a smartphone.

3.3 Operation and Results

The experiments were performed by using the experimental setup shown in Figure 3.9. The complete PV array setup, measurement circuit, a tablet, and a PC are connected with each other and various parameters are varied to observe their effects.

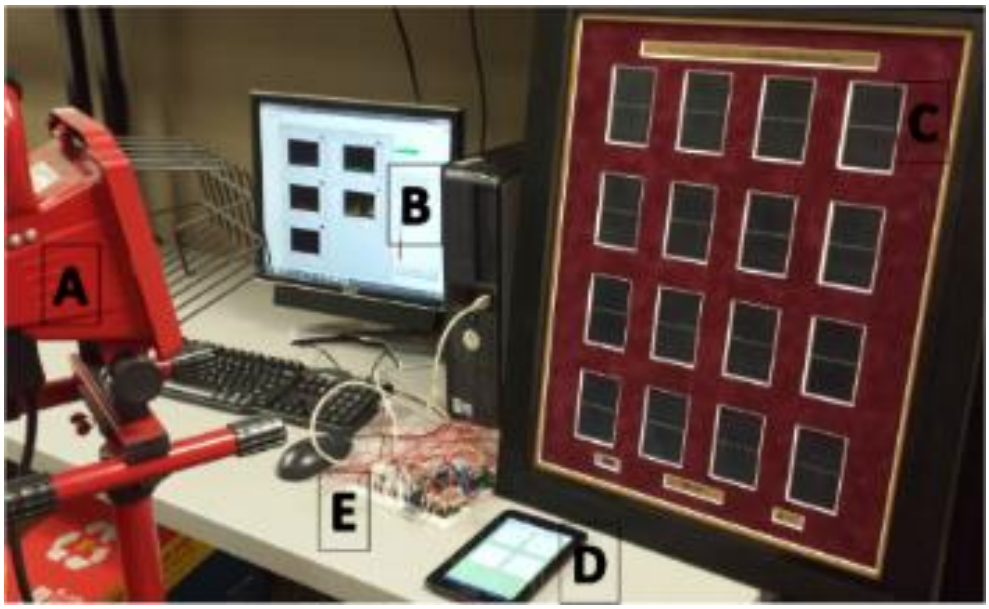

Figure 3.9 Complete Experimental Setup.

A) Halogen lamp B) LABVIEW on PC C) PV array setup D) Tablet with app E) Measurement circuit.

The I-V characteristic curve is plotted for a single solar panel and resulted in a curve nearly identical to the one provided on the manufacturer's data sheet (Figure 3.10). The slight deviations of the curve at the ends of the I-V curve are due to use of a low precision potentiometer which acts as a load to the solar panel. Similarly, the P-V characteristic is also plotted in Figure 3.10, with a red circle indicating the maximum power point of the panel.

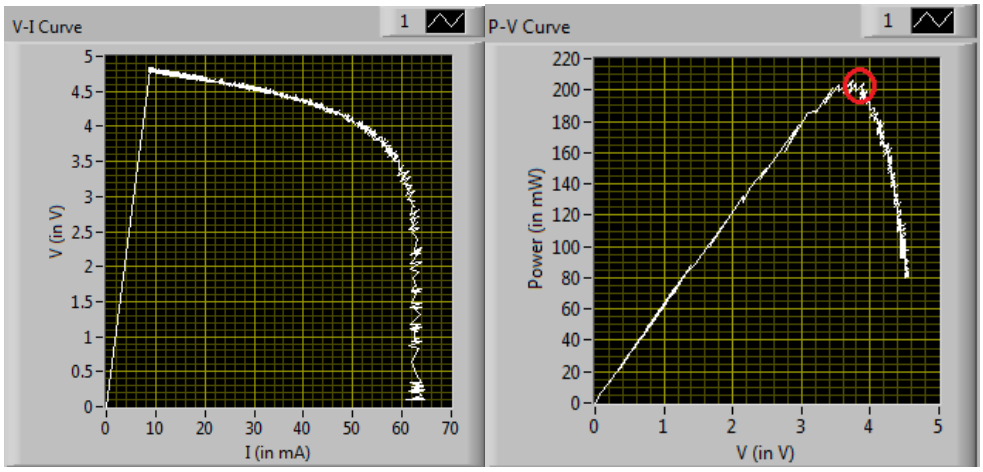

Figure 3.10 Characteristic V-I and P-V Curves of a Single Solar Panel.

Effect of Shading

Experiments to observe effect of shading were performed when single or multiple solar panels were shaded. As expected, the voltage across the series string dropped down if one of the panel was shaded as shown in Figure 3.11. But, the current remains the same for the series string.

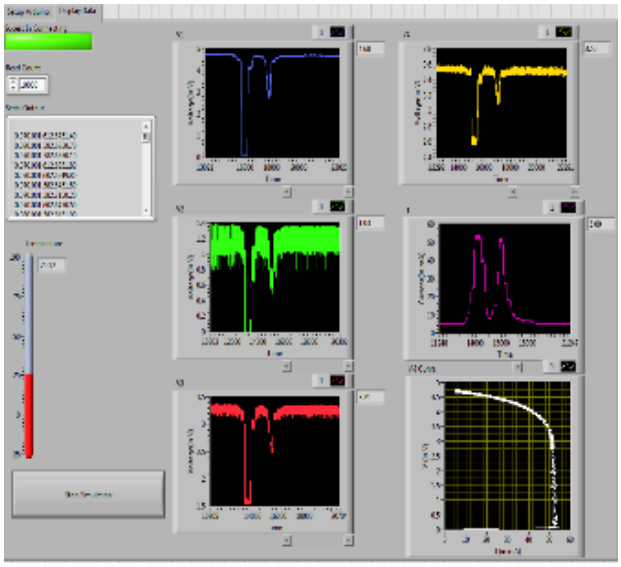

Figure 3.11 Effect of Shading.

Effect of Topology

Variation of topology, i.e. connections between multiple solar panels, was tested. It was observed that in parallel combination, the fault in a single solar panel would not affect the performance of other solar panels. However, in the case of series-parallel connection, a fault in a single solar panel causes the voltage across the whole series string to go down.

The output of the series string is limited by the current of the worst performing panel. The above effects can also be shown by using a scatter plot which include the sample I-V operating points of each solar panel. If the sample points are scattered (Figure 3.12), then it indicates that there is a fault in the PV array and if the points are clustered together, the array is working normally (Figure 3.13).

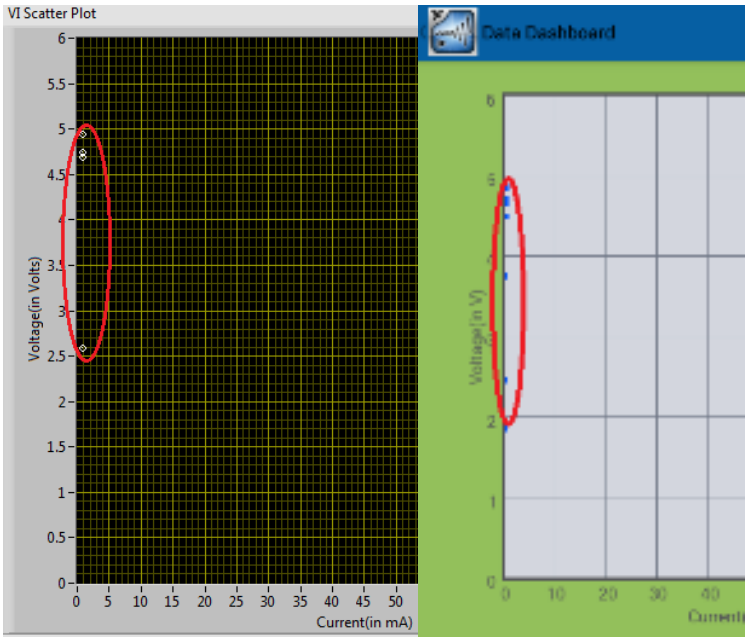

Figure 3.12 Scatter Plot for Faulty Operation.

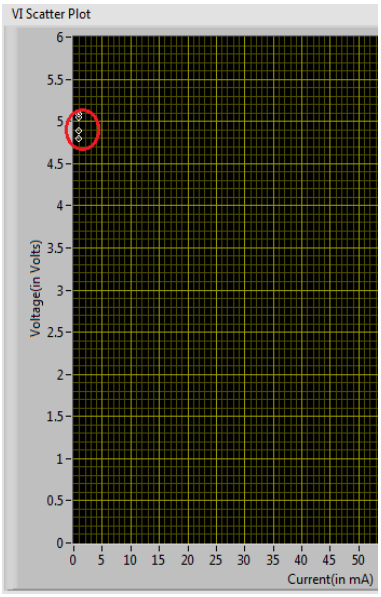

Figure 3.13 Scatter Plot for Normal Operation.

3.4 Android App Development

An easy to use custom android application to view the collected data is in development. Details of the app design are described in this section. On startup of the app, the user is prompted for the server address, and then a progress bar is displayed as it downloads the necessary data. The main interface consists of three display tabs. The first tab displays the power output, temperature, and irradiance of the array. The central graph displays the total power production, and each “slice” of the pie chart can be selected for additional information. The data of these figures can be real time data or average data over a time period according to user settings. The temperature and irradiance have a variety of icons (partial cloudy, sunny day, high temperature, low temperature) which adjust based on the value. The next tab, “Graph”, expands much of this information into a time series plot. The last tab a simplified electrical schematic of the array. The panel icons can be clicked to display unique information of each solar panel, such as real time

voltage, current, and power. Future features which will be added include a comparison of current power generation to the average, the theoretical predicted power, and the peak power for a period. The snapshots for the app in development are shown in Figure 3.14.

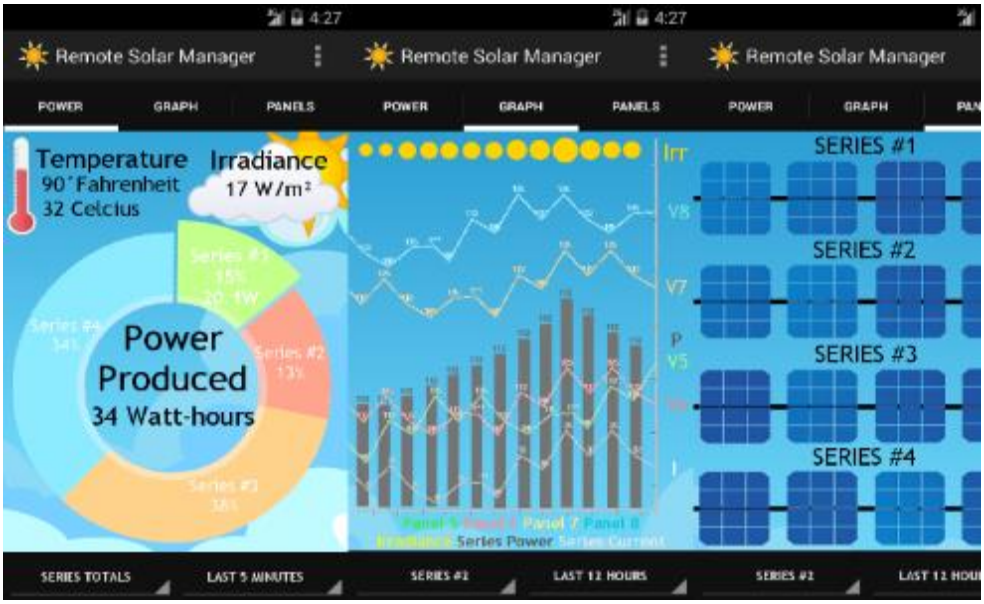

Figure 3.14 Snapshot of Custom Monitoring App.

Usefulness of the Simulator

The monitoring simulator is useful in capturing common faults in the system like shading, change of load, soiling, line to line fault and ground faults. There are many more faulty situations that can't be captured on the monitoring simulator like effect partial shading on a single solar panel, islanding, mismatch loss conditions, etc. This is due to limitation of small scale fixed configuration of the array as well as the use of a halogen lamp as virtual light source (it does not capture the complete spectrum of natural light). Although there are some limits to which simulator can be used, because of the ease of use and the compact size makes it suitable for lab usage.

Chapter 4

IRRADIANCE ESTIMATION FOR A SMART PV ARRAY

4.1 PV Array Under Partial Shading Conditions

We consider the problem of deriving a circuit model of a PV array under partial shading conditions, using only voltage, current, and temperature measurements from every module. Several factors complicate this task and make it non-trivial. Since measurements are taken on an active and functioning array, I-V curves from individual modules are not available. Also, since partial shading is present, we can no longer assume that module-level measurements are taken at the modules' maximum power point (MPP). This is because an inverter with maximum power point tracking (MPPT) will seek the array's maximum power point, causing some or all of the modules to operate away from their own MPP. Finally, shading affects not only the power of the incoming solar radiation, but its spectrum as well. Air mass models exist to predict the effect of changing solar spectral characteristics [137], but these typically assume light travels through clear, dry air.

4.2 The UW-Madison PV Circuit Model

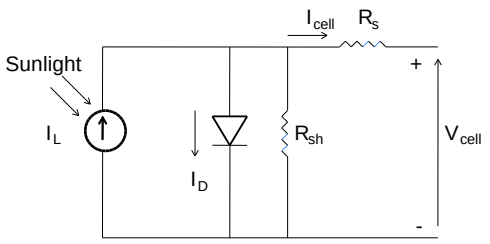

Figure 4.1 Single-Diode Model of PV Module with Parasitic resistances.

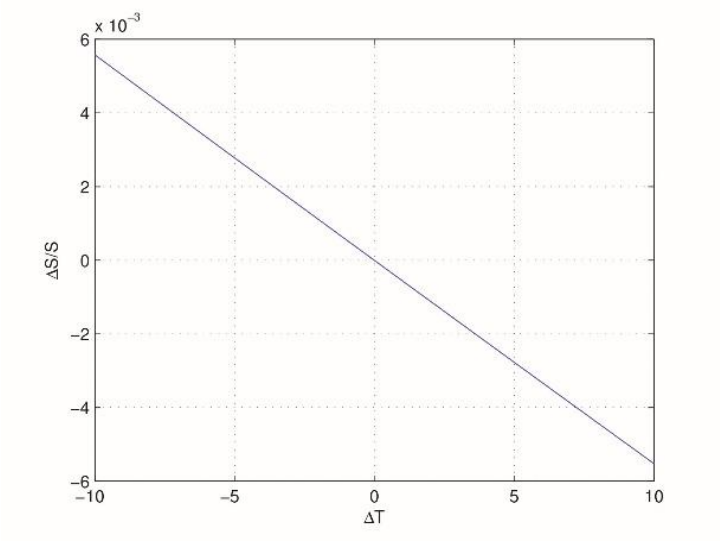

Figure 4.2 Normalized Error in Irradiance Estimates as a Function of Error in Temperature. Sharp NT-175U Module at Standard Reference Conditions and Maximum Power Point.

Multiple models exist to predict PV module behavior as a function of environmental conditions, including the Sandia model developed by King et al. [138] and the UW-Madison model developed by De Soto [139]. For the work described here, the UW- Madison model was chosen for several reasons. First and most importantly, it is acceptably accurate for modeling the behavior of crystalline silicon PV modules under a variety of conditions. Second, the model requires only the information from a manufacturer's data sheet, with no additional measurements needed. Finally, the model gives an explicit representation of a PV module as an electrical circuit (Fig 4.1), allowing easy simulation of arrays as soon as model parameters are determined. In contrast, the Sandia model is highly accurate, but depends on extensive measurements of modules beyond what is typically available from manufacturers and does not give an easily simulated circuit representation of a module.

The Single-Diode Circuit Model

The heart of the UW-Madison model is the single-diode PV Cell model with series and shunt (parallel) resistances, shown in Fig. 4.1. This model captures the essential behavior of conventional crystalline silicon PV models. The UW-Madison model extends the single-diode representation with a semi-empirical model of the variation in circuit parameters as environmental conditions change. The diode current I_D as a function of diode voltage V_D is given by the Shockley diode equation,

$$I_D = I_0(\exp[V_D] - 1) \tag{12}$$

where I_0 is the diode reverse saturation current and a is the modified ideality factor of the module, described below. a reflects more than the ideality factor of the P-N junction in the PV cell; it also includes the effect of temperature and the fact that PV modules contain many cells in series. “a” is defined as

$$a = \frac{N_s n_1 k_b T_c}{q} \tag{13}$$

where Tc is the absolute cell temperature, k_b is the Boltzmann constant, q is the electron charge, n_1 is the ideality factor as it is usually defined, and Ns is the number of cells in series. n_1 typically takes values between 1 and 2, while N_S typically takes values on the order of 10-100 cells, leading to a diode with a threshold voltage in the tens of volts.

This diode model leads to the following transcendental equation for module current I as a function of module voltage V:

$$I = I_L - I_0\left(exp\left[\frac{V+IR_s}{a}\right] - 1\right) - \frac{V+IR_s}{R_{sh}} \tag{14}$$

Variation with Environmental Conditions

The single-diode PV cell model described in previous section determines the behavior of a PV module at the manufacturer's specified operating conditions. The UW-Madison model extends this representation by defining the values of the circuit parameters as environmental conditions vary. Current I_L in (14) varies as a function of incoming irradiance S, air mass A, and cell temperature T_C. Its behavior is given by

$$I_L = \frac{S}{S_{ref}} f_1(M)\left[I_{L,ref} + \alpha_{I_{SC}}\left(T_C - T_{C,ref}\right)\right] \quad (15)$$

where S_{ref}, M_{ref}, and T_{ref} are the values of irradiance, air mass, and temperature at the manufacturer's reference conditions. α_{ISC} is the temperature coefficient of short circuit current, given by the manufacturer. $f_1(M)$ is the air mass modifier and is common to all modules of the same type (e.g. crystalline silicon). f_1 has been determined empirically in [138].

The diode behavior is affected by both the temperature dependence in (13) and by changes in I_0. I_0 is dependent on temperature through changes in the density of charge carriers and changes in the band gap of the material. This dependence is modeled as

$$I_0 = I_{0,ref}\left(\frac{T_C}{T_{C,ref}}\right)^3 exp\left[\left(\frac{E_{g,ref}}{T_{C,ref}} - \frac{E_g}{T_C}\right)\left(\frac{q}{k_b}\right)\right] \quad (16)$$

$$E_g = E_{g,ref}\left[1 - 0.0002677\left(T_C - T_{C,ref}\right)\right] \quad (17)$$

where E_g is the material's band gap and $I_{0,ref}$, $T_{c,ref}$, and $E_{g,ref}$ are the values of I_0, T_C, and E_g at reference conditions. The parasitic resistance R_s and R_{sh} are modeled as follows. R_S

is found to have a minimal effect on the I-V curve and is assumed constant at its reference value. R_{sh} is modeled as being inversely proportional to incoming irradiance:

$$R_{sh} = R_{sh,ref}\frac{S_{ref}}{S} \tag{18}$$

Taken together, (12), (15), and (18) define a circuit model for the PV module under all operating conditions.

4.3 Irradiance Estimation Procedure

The PV array model described in Section 4.2 can be used to derive a method for estimating the irradiance S from measurements of I, V, and T_C. Solving the system of (14), (15), and (18) for S yields the expression

$$S = S_{ref}\left(\frac{I+I_0\left(exp\left[\frac{V+IR_S}{a}\right]-1\right)}{f_1(M)\left[\alpha_{I_{SC}}\left(T_C-T_{C,ref}\right)\right]-\frac{V+IR_S}{R_{sh,ref}}}\right) \tag{19}$$

4.4 Sources of Error

The irradiance estimation procedure described in Section 4.3 is clearly accurate when V, I, M, and T_C are perfectly known and the model perfectly matches the behavior of the device. However, none of these conditions holds true in practice: measurements are always noisy and the UW-Madison model is only an approximation of device behavior. Furthermore, cell temperature T_C in our implementation is estimated from module back-surface temperature. King gives a model [138] for estimating the temperature difference between cell and module back surface temperatures, but this is of course not perfectly accurate. Finally, Air mass M is typically calculated based on the solar zenith angle [137] but these functions are unlikely to be accurate under partial shading conditions. The

source and intensity of shade (e.g. clouds vs. buildings) will affect air mass in ways that cannot be feasibly predicted by any method we are aware of. This section examines the effects of several potential sources of error on the accuracy of estimated irradiance S, and maximum power current, voltage, and power I_{MP}, V_{MP}, P_{MP}.

Measurement Noise

The relationship between noise in model inputs and error in output is extremely important, but the complex and non-linear input/output relationship makes evaluating these effects non-trivial. We examine this important relationship between input noise and output error using the widely used first-order propagation of error equation. Assuming statistical independence between sources of error, this relationship is given by

$$var\big(f(x,y,z,\dots)\big) \approx \frac{\partial^2}{\partial x}(\sigma_x^2) + \frac{\partial^2}{\partial y}\big(\sigma_y^2\big) + \frac{\partial^2}{\partial z}(\sigma_z^2) + \cdots \tag{20}$$

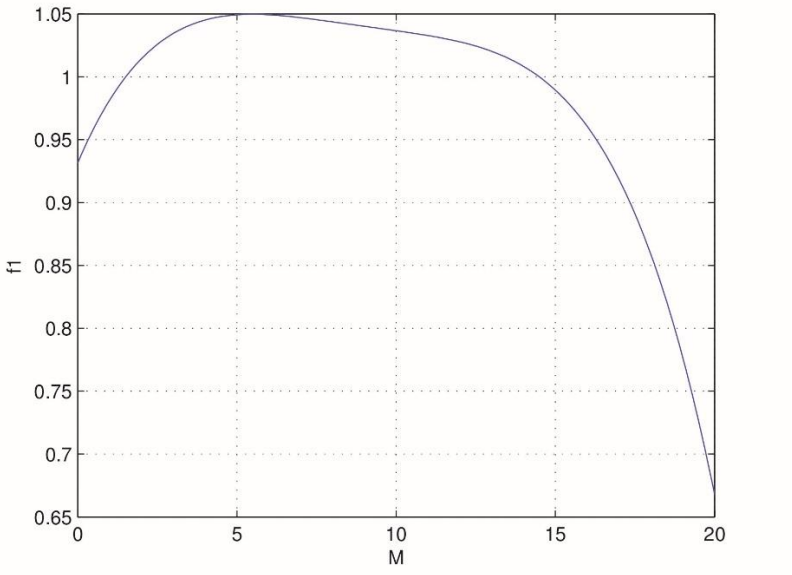

Figure 4.3 Airmass Factor $f_1(m)$.

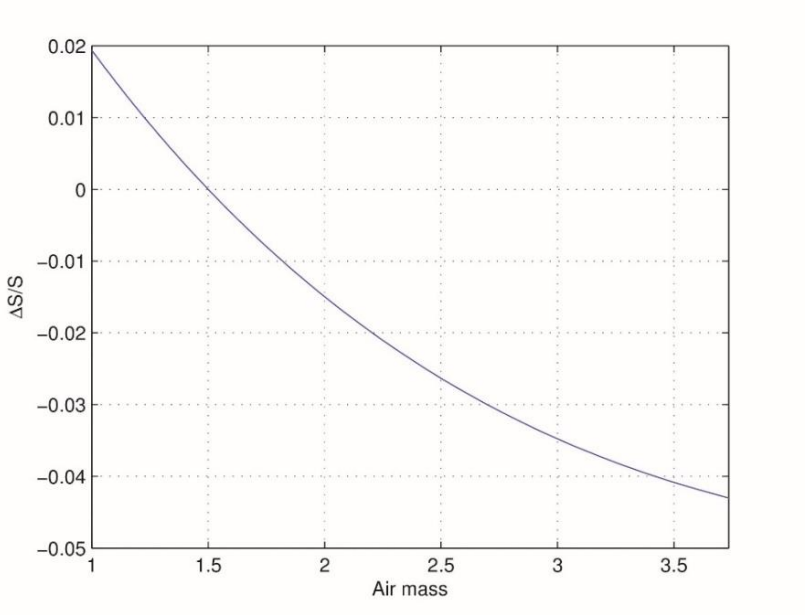

Figure 4.4 Normalized Error in Estimated Irradiance for Varying Air Mass for Sharp NT-175U1 Module, Other Parameters held at STC.

Evaluating each partial derivative in (20), we arrive at the following expressions.

$$\frac{\partial}{\partial T_c}\left(\frac{S}{S_{ref}}\right) = \frac{I_0\left[exp\left[\frac{(V+IR_s)q}{N_s n_1 k_b T_c}\right]\left(\frac{3T_C^2}{T_{C,ref}^3} - \frac{(V+IR_s)q}{N_s n_1 k_b T_C^2} + \frac{E_q}{T_C^2}\frac{q}{k_b}\right)\right]}{f_1(M)\left[\alpha_{I_{SC}}\left(T_C - T_{C,ref}\right)\right] - \frac{V+IR_s}{R_{sh,ref}}}$$

$$- \frac{\left[I + I_0\left(exp\left[\frac{(V+IR_S)q}{N_S n_1 k_b T_C}\right] - 1\right)\right] f_1(M)\alpha_{I_{SC}}}{\left[f_1(M)\left[\alpha_{I_{SC}}\left(T_C - T_{C,ref}\right)\right] - \frac{V+IR_S}{R_{sh,ref}}\right]^2} \tag{21}$$

$$\frac{\partial}{\partial I}\left(\frac{S}{S_{ref}}\right) = \frac{1 + I_0\frac{R_s}{a}exp\left[\frac{V+IR_s}{a}\right]}{f_1(M)\left[\alpha_{I_{SC}}\left(T_C - T_{C,ref}\right)\right] - \frac{V+IR_s}{R_{sh,ref}}}$$

$$- \frac{R_S/R_{sh,ref}\left[I + I_0\left(exp\left[\frac{V+IR_S}{a}\right] - 1\right)\right]}{\left[f_1(M)\left[\alpha_{I_{SC}}\left(T_C - T_{C,ref}\right)\right] - \frac{V+IR_S}{R_{sh,ref}}\right]^2} \tag{22}$$

$$\frac{\partial}{\partial V}\left(\frac{S}{S_{ref}}\right) = \frac{\frac{I_0}{a}\,exp\left[\frac{V+IR_s}{a}\right]}{f_1(M)\left[\alpha_{I_{SC}}\left(T_C - T_{C,ref}\right)\right] - \frac{V+IR_s}{R_{sh,ref}}}$$

$$- \frac{1/R_{sh,ref}\left[I + I_0\left(exp\left[\frac{V+IR_s}{a}\right] - 1\right)\right]}{\left[f_1(M)\left[\alpha_{I_{SC}}\left(T_C - T_{C,ref}\right)\right] - \frac{V+IR_s}{R_{sh,ref}}\right]^2} \tag{23}$$

The following sections further explore the robustness of the algorithm.

Air Mass

Absorption and scattering of light by the atmosphere changes the spectrum of incoming radiation, which in turn affects the output power of a PV cell. The air mass environmental parameter is used to model this effect. Air mass M is a dimensionless quantity representing the number of atmospheres light must travel through in order to reach the module. Orbiting satellites receive radiation with M=0, while a module at sea level with the sun directly overhead receives M=1. Air mass 1.5 has been arbitrarily chosen as a typical value, balancing the low airmass of midday with the higher air mass experienced when the sun is at a lower angle. In the PV performance models considered here, the air mass modifier $f_1(M)$ summarizes the effect of changing air mass on power output. $f_1(M)$ is a fourth-degree polynomial with empirically determined coefficients:

$$f_1(M) = a_0 + a_1 M + a_2 M^2 + a_3 M^3 + a_4 M^4 \tag{24}$$

Figure 4.3 shows King et al.'s values for $f_1(M)$ for a typical crystalline silicon PV module, with airmass ranging from 1 to 35, corresponding to solar zenith angles of approximately 0 to 90 degrees. The air mass modifier is potentially problematic for the irradiance estimation procedure presented here, since the effect of partial shading on the

spectrum of incoming light is unknown. However, the air mass modifier $f_1(M)$ is very near 1 for air mass $1<M<4$. The vast majority of available solar energy arrives at a zenith angle of 75 degrees or less, indicating that the effect of air mass can be neglected without destroying the fidelity of the estimation, at least as far as modeling of partial shading is concerned. Figure 4.4 shows the effect of error in airmass on estimated irradiance at STC. Note that if an airmass of 1.5 is assumed by the algorithm, an irradiance error of only approximately 4% is observed, even if actual airmass is a relatively large value of 3.5.

Temperature Bias

Module back surface temperature measurements are easy to acquire, but do not accurately represent the cell temperature. A reasonably accurate method has been proposed to estimate cell temperature [140], but this remains a potential source of error for the irradiance estimation algorithm. Persistent temperature errors of up to 4◦ C may occur.

A first-order description of the relationship between temperature bias and error has already been given in Section 4.4. Figure 4.2 extends this model by plotting the error in irradiance as a function of the error in temperature bias at STC (standard test conditions), as well as three other temperature and irradiance conditions. Temperature errors of 4 degrees or less produce at most a 0.2% error in estimated irradiance, corresponding to an error of only 2 W/m^2. In a mismatch mitigation application this is an acceptable level of error.

Chapter 5

CONCLUSIONS AND FUTURE WORK

The third chapter considers a PV array monitoring system where smart sensors are attached to the PV modules and transmit data to a monitoring station through wireless links. These smart monitoring devices can be used for fault detection and management of connection topologies. And, a compact hardware simulator of the smart PV array monitoring system is described. The voltage, current, irradiance, and temperature of each PV module are monitored and the status of each panel along with all data is transmitted to a mobile device. The system is implemented with an Arduino board to measure, record and analyze data from multiple sensors connected to a series-parallel configuration 4x4 PV array system. LABVIEW and Arduino board programs have been developed to display and visualize the monitoring data from sensors. The simulator was successfully tested for demonstrations in a laboratory environment. Various PV array conditions including shading, faults, and loading are simulated and demonstrated. All data is saved on servers and mobile devices and desktops can easily access analytics from anywhere. The smartphone app has also made the system data accessible from anywhere on any device. Improvements can be achieved by customizing the smartphone app so that a technician can easily decipher the information and check for faults in the system. Finally, our implementation can also be used for educational purposes in classrooms, where students can observe and better understand the operation of PV arrays.

In the fourth chapter, the algorithm presented accurately estimates circuit parameters when air mass and cell temperature are known and measurements are accurate, Further, it

shows graceful degradation when measurements are noisy. While the irradiance estimation method shows sufficiently good performance to be useful, there are several potential improvements. This method is not known to be optimal. To this end, work is in progress to formulate and solve the problem in a Bayesian framework. This would allow several desirable behaviors, such as automatically rejecting irradiance values greater than what is possible from full sun. This would be especially useful for modules operating at higher voltages than V_{MP}, where estimation is expected to become less accurate. Another effect which should be taken into account is the presence of bypass diodes in each module. Under sufficient shading, a PV module becomes reverse biased and a diode activates to protect the module and conduct excess current beyond the module's short circuit current I_{SC}. Also, this presents potential problems for the estimator, since it was developed without regard for the presence of bypass diodes. However, we believe that larger errors due to the action of bypass diodes are only mildly problematic, since the primary purpose of the algorithm is to identify shaded modules; this task is relatively trivial if shading is severe enough to activate bypass diodes. In this case, our method's estimated irradiance is expected to act as an upper bound on the module's actual irradiance. In spite of these shortcomings, however, the irradiance estimation procedure serves its intended purpose. Errors under 5% are unlikely to result in incorrect decisions regarding array electrical configuration. As part of a larger system of array monitoring and control, the method presented here allows for increased power output under partial shading conditions.

REFERENCES

[1] Robert L. San Martin, Solar energy (Access Science, McGraw-Hill Companies, 2008).

[2] Renewables Global Status Report (REN21, 2014).

[3] J. Conti and P. Holtberg, “Levelized cost of new generation resources in the annual energy outlook 2011,” US Energy Information Administration, Tech. Rep., Dec. 2010

[4] M. Begovic, S. Ghosh, and A. Rohatgi, “Decade performance of a roof-mounted photovoltaic array,” IEEE 4th World Conference on Photovoltaic Energy Conversion, vol. 2, pp. 2383 –2386, May 2006.

[5] Y. Zhao, J. F. de Palma, J. Mosesian, R. Lyons, and B. Lehman, “Line-line fault analysis and protection challenges in solar photovoltaic arrays," IEEE Transactions on Industrial Electronics, vol. 60, no. 9, pp. 3784-3795, Sept 2013.

[6] S. Harb and R. Balog, “Reliability of candidate photovoltaic module integrated-inverter (PV-MII) topologies-a usage model approach," IEEE Transactions on Power Electronics, vol. 28, no. 6, pp. 3019-3027, June 2013.

[7] A. D. Hansen, P. Sorensen, L. H. Hansen, & H. Bindner, “Models for a Stand-Alone PV System,” Riso National Laboratory, Roskilde, December, 2000, 11-12, ISBN 87-550-2776-8.

[8] Laurent Mingo, “A Cost-effective Solution for Photovoltaic Panels Performance Monitoring Using NI LabVIEW”, Blue System Integration Ltd., www.bluesystem.ca.

[9] Dimitris Ipsakisa, Spyros Voutetakisa, Panos Seferlisa, Fotis Stergiopoulosa, & Costas Elmasidesb, “Power management strategies for a stand-alone power system using renewable energy sources and hydrogen storage”, International journal of hydrogen energy, vol 34, pp. 7081–7095, 2009.

[10] M.B. Zahran, & O.A. Mahgoub, “Photovoltaic Battery (PVB) Stand-alone System Control Signals Estimation”, Proc. World Renewable Energy Congress VI, 2000, pp. 2119–2122.

[11] Mohammad Zakir Hossain, & A.K.M. Sadrul Islam, “PV wind Hybrid System Modelling for Remote Rural Application”, ISESCO Science and Technology Vision, vol. 3(4), November 2007, 59-64.

[12] K.Otani, T.Takashima, and K.Kurokawa, “Performance and reliability of 1MWphotovoltaic power facilities in AIST,”, IEEE 4thWorld Conference on Photovoltaic Energy Conversion, vol. 2, May 2006, pp. 2046–2049.

[13] P.S.Dahl, A PC and Lotus-based data acquisition/reduction system for an ICP spectrometer, Comput. Geosci, 16(7), 2000, 881–892.

[14] D. King,W. Boyson, and J. Kratochvil, “Analysis of factors influencing the annual energy production of photovoltaic systems,” In Proc. Conference Record of the Twenty-Ninth IEEE Photovoltaic Specialists Conference, 2002., pp. 1356 – 1361, 2002.

[15] T. Nordmann and L. Clavadetscher, “Understanding temperature effects on PV system performance,” Proceedings of 3rd World Conference on Photovoltaic Energy Conversion, 2003., vol. 3, pp. 2243 –2246, 2003.

[16] D. L. King, J. Kratochvil, and W. Boyson, “Measuring solar spectral and angleof-incidence effects on photovoltaic modules and solar irradiance sensors,” Conference Record of the Twenty-Sixth IEEE Photovoltaic Specialists Conference, 1997., pp. 1113–1116, 1997.

[17] J. Nelson, The Physics of Solar Cells. Imperial College Press, 2003.

[18] C. Honsberg and S. Bowden, PV CDROM. [Online]. Available: http://www.pveducation.org/pvcdrom.

[19] W. De Soto, S. Klein, and W. Beckman, “Improvement and validation of a model for photovoltaic array performance,” Solar Energy, vol. 80, no. 1, pp. 78 – 88, Aug. 2006.

[20] M. El-Shibini and H. Rakha, “Maximum power point tracking technique,” in Electrotechnical Conference, 1989. Proceedings. ‘Integrating Research, Indus-60try and Education in Energy and Communication Engineering’, MELECON ’89., Mediterranean, 1989, pp. 21 –24.

[21] F. Baumgartner, H. Scholz, A. Breu, and S. Roth, “MPP voltage monitoring to optimize grid connected system design rules,” in Proceedings 19th European Photovoltaic Solar Energy Conference, June, 2004, pp. 7–11.

[22] I. Altas and A. Sharaf, “A novel on-line MPP search algorithm for PV arrays,” Energy Conversion, IEEE Transactions on, vol. 11, no. 4, pp. 748 –754, Dec.1996.

[23] A. Al-Amoudi and L. Zhang, “Application of radial basis function networks for solar-array modelling and maximum power-point prediction,” Generation, Transmission and Distribution, IEEE Proceedings, vol. 147, no. 5, pp. 310 –316, Sep. 2000.

[24] F. Spertino and J. Akilimali, “Are manufacturing I-V mismatch and reverse currents key factors in large photovoltaic arrays,” IEEE Transactions on Industrial Electronics,, vol. 56, no. 11, pp. 4520 –4531, Nov. 2009.

[25] R. Hammond, D. Srinivasan, A. Harris, K. Whitfield, and J.Wohlgemuth, “Effects of soiling on PV module and radiometer performance,” Conference Record of the Twenty-Sixth IEEE Photovoltaic Specialists Conference, pp. 1121 –1124,1997.

[26] H. Patel and V. Agarwal, “MATLAB-Based modeling to study the effects of partial shading on PV array characteristics,” IEEE Transactions on Energy Conversion, vol. 23, no. 1, pp. 302 –310, Mar. 2008.

[27] D. Nguyen and B. Lehman, “Modeling and simulation of solar PV arrays under changing illumination conditions,” In Proc. IEEE Workshops on Computers in Power Electronics, 2006. COMPEL ’06., pp. 295 –299, July 2006.

[28] V. Quaschning and R. Hanitsch, “Numerical simulation of current-voltage characteristics of photovoltaic systems with shaded solar cells,” Solar Energy, vol. 56, no. 6, pp. 513-520, 1996.

[29] NFPA 70: National Electrical Code, NFPA Std., 2008.

[30] G. Gregory and G. Scott, “The arc-fault circuit interrupter: an emerging product,” IEEE Transactions on Industry Applications, vol. 34, no. 5, pp. 928 –933, 1998.

[31] H. Haeberlin and M. Kaempfer, “Measurement of damages at bypass diodes by induced voltages and currents in PV modules caused by nearby lightning currents with standard waveform,” 23rd European Photovoltaic Solar Energy Conference, 2008.

[32] C. Deline, “Partially shaded operation of a grid-tied PV system,” 34th IEEE Photovoltaic Specialists Conference (PVSC), June 2009, pp. 268-273.

[33] B. Brooks, “The bakerseld - a lesson in ground-fault protection", SolarPro Magazine, pp. 62-70, 2011.

[34] P. Jackson, “Target roof PV Fire of 4-5-09, 9100 Rosedale highway, Bakerseld, California," City of Bakerseld, CA Development Services/Building Department Memorandum, pp. 4-29, 2009.

[35] G. Velasco, J. Negroni, F. Guinjoan, and R. Pique, “Irradiance equalization method for output power optimization in plant oriented grid-connected PV generators,” European Conference on Power Electronics and Applications, 2005, p. 10.

[36] S. T. Buddha, H. Braun, V. Krishnan, C. Tepedelenlioglu, A. Spanias, T. Yeider, and T. Takehara, "Signal processing for photovoltaic arrays," International Conference on Emerging Signal Processing Applications, Jan 2012.

[37] H. Braun, S. T. Buddha, V. Krishnan, A. Spanias, C. Tepedelenlioglu, T. Yeider, & T. Takehara, "Signal processing for fault detection in photovoltaic arrays", Proc. of IEEE International Conference on Acoustics, Speech and Signal Processing (ICASSP), pp. 1681-1684, March 2012.

[38] G. Farivar, B. Asaei, N. Haghdadi, and H. Iman-Eini, "A novel temperature estimation method for solar cells," 2nd. IEEE Power Electronics, Drive Systems and Technologies Conference (PEDSTC), 2011, pp. 336–341.

[39] N. Forero, J. Hernández, & G. Gordillo, "A Development of a monitoring system for a PV solar plant", Energy Conversion and Management, 2006, vol. 47, 2329-2336.

[40] E. Román, R. Alonso, P. Ibañez, S. Elorduizapatarietxe, & D. Goitia, "Intelligent PV module for grid-connected PV systems", IEEE Transactions on Industrial Electronics, 2006, 53(4), 1066-1073.

[41] U. Jahn, & W. Nasse, "Operational performance of grid connected PV systems on buildings in Germany", Proc. Progress in Photovoltaic: Research and Applications,2004, 12, 2004, 441-448.

[42] Lab View-the software that powers virtual instrumentation (National Instrument, 2008).

[43] K. N. Ramamurthy, J. J. Thiagarajan, & A. Spanias, "An Interactive Speech Coding Tool using LabVIEW", Proc. of IEEE DSP Workshop, Sedona, Jan. 2011, 180-185.

[44] A. Spanias, "Digital Signal Processing: An Interactive Approach – 2nd Edition", Lulu Press On-demand Publishers, Morrisville, NC, ISBN 978-1-4675-9892-7, May 2014.

[45] Measurement of photovoltaic current-voltage characteristic (International Electrotechnical Commission), IEC 60904(1), 2006.

[46] H. Braun, S. T. Buddha, V. Krishnan, A. Spanias, C. Tepedelenlioglu, T. Yeider, & T. Takehara, "Signal processing for fault detection in photovoltaic arrays", Proc. IEEE International Conference on Acoustics, Speech and Signal Processing (ICASSP), 1681-1684, March 2012, 25-30.

[47] H. Braun, S. T. Buddha, V. Krishnan, A. Spanias, C. Tepedelenlioglu, T. Yeider, T. Takehara, & S. Takada, "Signal Processing for Solar Array Monitoring, Fault Detection, and Optimization", Morgan and Claypool eBooks, ISBN 978-1608459483, 2012.

[48] F. Kasten and A. T. Young, “Revised optical air mass tables and approximation formula,” Applied Optics, 28(22), pp. 4735–4738, Nov 1989.

[49] A. Drews, A.C. de Keizer, H.G. Beyer, E. Lorenz, J. Betcke, W. van Sark, W. Heydenreich, E. Wiemken, S. Stettler, P. Toggweiler, S. Bofinger, M. Schneider, G. Heilscher, D. Heinemann. “Monitoring and remote failure detection of grid-connected PV systems based on satellite observations”, Solar Energy, 81 (4), 2007, pp. 548–564

[50] S. Silvestre, A. Chouder, and E. Karatepe, “Automatic fault detection in grid connected PV systems," Solar Energy, vol. 94, pp. 119-127, 2013.

[51] W. Zhou, H. Yang, Z. Fang, “A novel model for photovoltaic array performance prediction”, Applied Energy, 2007, 84(12), pp. 1187–1198.

[52] A. Chouder, S. Silvestre, “Analysis Model of Mismatch Power Losses in PV Systems”, Journal of Solar Energy Engineering, 2009, Vol. 131, 024504-(1-5).

[53] E. Meyer and E. Ernest van Dyk, “Assessing the reliability and degradation of photovoltaic module performance parameters," IEEE Transactions on Reliability, vol. 53, no. 1, pp. 83-92, 2004.

[54] S. Vergura, G. Acciani, V. Amoruso, and G. Patrono., “Inferential statistics for monitoring and fault forecasting of PV plants,” IEEE International Symposium on Industrial Electronics, 2008, pages 2414–2419.

[55] S. Vergura, G. Acciani, V. Amoruso, G. E. Patrono, and F. Vacca, “Descriptive and inferential statistics for supervising and monitoring the operation of PV Plants,” IEEE Transactions on Energy Conversion in Industrial Electronics, 56(11):4456–4464, 2009.

[56] A. Abete, E. Barbisio, P. Cane, and P. Demartini, “Analysis of photovoltaic modules with protection diodes in presence of mismatching," 21st IEEE Photovoltaic Specialists Conference, May 1990, vol.2, pp. 1005-1010.

[57] D. Stellbogen, “Use of PV circuit simulation for fault detection in PV array fields," Proc. 23rd IEEE Photovoltaic Spec. Conf., 1993, pp. 1302-1307.

[58] M. Miwa, S. Yamanaka, H. Kawamura, H. Ohno, and H. Kawamura, “Diagnosis of a power output lowering of PV array with a (-dI/dV)-V characteristic," 2006 IEEE 4th World Conference on Photovoltaic Energy Conversion, May 2006, vol. 2, pp. 2442-2445.

[59] P. Hernday, “Field Applications for I-V Curve Tracers," SolarPro Magazine, Issue 4.5, Aug/Sep, pp. 77-106, 2011.

[60] A. Drews, A. de Keizer, H. Beyer, E. Lorenz, J. Betcke, W. van Sark, W. Heydenreich, E. Wiemken, S. Stettler, P. Toggweiler, S. Bonger, M. Schneider, G.

Heilscher, and D. Heinemann, “Monitoring and remote failure detection of grid-connected PV systems based on satellite observations," Solar Energy, 81(4), pp. 548 - 564, 2007.

[61] “International standard IEC 61724: Photovoltaic system performance monitoring - Guidelines for measurements, data exchange and analysis," 1998.

[62] B. Marion, J. Adelstein, K. Boyle, H. Hayden, B. Hammond, T. Fletcher, B. Canada, D. Narang, A. Kimber, L. Mitchell, G. Rich, and T. Townsend, “Performance parameters for grid-connected PV systems," 31st IEEE Photovoltaic Specialists Conference, Jan 2005, pp. 1601-1606.

[63] H. Haeberlin and C. Beutler, “Normalized representation of energy and power for analysis of performance and on-line error detection in PV-systems," 13th EU PV Conference on Photovoltaic Solar Energy Conversion, 1995.

[64] D. Nguyen, B. Lehman, and S. Kamarthi, “Performance evaluation of solar photovoltaic arrays including shadow effects using neural network," in IEEE Energy Conversion Congress and Exposition, 2009, pp. 3357-3362.

[65] D. Riley and J. Johnson, “Photovoltaic prognostics and heath management using learning algorithms," 38th IEEE Photovoltaic Specialists Conference (PVSC), June 2012, pp. 001(535)-001(539).

[66] S. Syafaruddin, E. Karatepe, and T. Hiyama, “Controlling of artificial neural network for fault diagnosis of photovoltaic array," 16th International Conference on Intelligent System Application to Power Systems (ISAP), 2011, pp. 1-6.

[67] A. M. Pavan, A. Mellit, D. D. Pieri, and S. Kalogirou, “A comparison between BNN and regression polynomial methods for the evaluation of the effect of soiling in large scale photovoltaic plants," Applied Energy, 108(0), pp.392-401, 2013.

[68] Y. Zhao, L. Yang, B. Lehman, J. F. de Palma, J. Mosesian, and R. Lyons, “Decision tree-based fault detection and classification in solar photovoltaic arrays," 27th Annual IEEE Applied Power Electronics Conference and Exposition (APEC), 2012, pp. 93-99.

[69] “B. Hu, Solar panel anomaly detection and classification,” Master thesis, 2012.

[70] Y. Zhao, R. Ball, J. Mosesian, J.F. de Palma and B. Lehman, “Graph-based Semi-Supervised Learning for Fault Detection and Classification in Solar Photovoltaic Arrays," IEEE Transactions on Power Electronics, 30(5), pp.2848-2858, 2015.

[71] B. Ando, S. Baglio, A. Pistorio, G.M. Tina, C. Ventura, “Sentinella: Smart Monitoring of Photovoltaic Systems at Panel Level,” IEEE Transactions on Instrumentation and Measurement, vol. 64, pp. 2188 – 2199, 2015.

[72] H. Braun, S. Buddha, V. Krishnan, A. Spanias, C. Tepedelenlioglu, T. Yeider, and T. Takehara, “Signal processing for fault detection in photovoltaic arrays," IEEE International Conference on Acoustics, Speech and Signal Processing (ICASSP), 2012, pp. 1681-1684.

[73] Y. Zhao, B. Lehman, R. Ball, J. Mosesian, and J.-F. de Palma, “Outlier detection rules for fault detection in solar photovoltaic arrays," Twenty-Eighth Annual IEEE Applied Power Electronics Conference and Exposition (APEC), 2013, pp. 2913-2920.

[74] B.-K. Kang, S.-T. Kim, S.-H. Bae, and J.-W. Park, “Diagnosis of output power lowering in a PV array by using the Kalman-filter algorithm," IEEE Transactions on Energy Conversion, 27(4), pp. 885-894, Dec 2012.

[75] X. Lin, Y. Wang, D. Zhu, N. Chang, and M. Pedram, “Online fault detection and tolerance for photovoltaic energy harvesting systems,” Proc. of the International Conference on Computer-Aided Design, 2012, pp. 1–6. ACM.

[76] Sunil Rao, David Ramirez, Henry Braun, Jongmin Lee, Cihan Tepedelenlioglu, Elias Kyriakides, Devarajan Srinivasan, Jeff Frye, Shinji Koizumi, Yoshitaka Morimoto and Andreas Spanias, “An 18kW Solar Array Research Facility for Fault Detection Experiments,” IEEE Mediterranean Electrotechnical Conference, April 2016.

[77] Deline C, Dobos A, Janzou S, Meydbray J, Donovan M. “A simplified model of uniform shading in large photovoltaic arrays,” Solar Energy, 2013, 96:274–82.

[78] García MC, Herrmann W, W. Bömer, B. Proisy, “Thermal and electrical effects caused by outdoor hot-spot testing in associations of photovoltaic cells,” Prog. Photovoltaics: Research and Applications, Vol. 11, 2003, pp. 293–307.

[79] Giaffreda D, Omana M, Rossi D., Metra C., “Model for thermal behavior of shaded photovoltaic cells under hot-spot condition,” IEEE international symposium on Defect and fault tolerance in VLSI and nanotechnology systems (DFT), 2011.

[80] Spagnolo GS, Del Vecchio P, Makary G, Papalillo D, Martocchia A, “A review of IR thermography applied to PV systems,” Eleventh international conference on Environment and electrical engineering (EEEIC), 2012.

[81] Herrmann W, Wiesner W, Vaassen W, “Hot spot investigations on PV modules-new concepts for a test standard and consequences for module design with respect to bypass diodes,” 26th IEEE Photovoltaic specialists conference, 1997.

[82] Meyer EL, van Dyk EE, “Assessing the reliability and degradation of photovoltaic module performance parameters” IEEE Transactions on Reliability, 2004;53 (1):83–92.

[83] Candela R, di Dio V, Sanseverino ER and Romano P, “Reconfiguration techniques of partial shaded PV systems for the maximization of electrical energy production,” International conference on clean electrical power; 2007, pp. 716–719.

[84] Silvestre S, Boronat A, Chouder A, “Study of bypass diodes configuration on PV modules,” Applied Energy 2009; 86(9):1632–40.

[85] Gokmen N, Karatepe E, Ugranli F and Silvestre S, “Voltage band based global MPPT controller for photovoltaic systems,” Solar Energy, 2013;98:322–34.

[86] Maki A, Valkealahti S, “Power losses in long string and parallel connected short strings of series-connected silicon-based photovoltaic modules due to partial shading conditions,” IEEE Transactions on Energy Conversion, 2012;27(1):173–83.

[87] Ramos-Paja C, Bastidas J, Saavedra-Montes A, Guinjoan-Gispert F, Goez M, “Mathematical model of TCT photovoltaic arrays in mismatching conditions,” IEEE fourth Colombian workshop on Circuits and Systems (CWCAS), 2012.

[88] Di Dio V, La Cascia D, Miceli R., Rando C, “A mathematical model to determine the electrical energy production in photovoltaic fields under mismatch effect,” International Conference on Clean Electrical Power, pp. 46–51, 2009.

[89] Skoplaki E, Palyvos J., “On the temperature dependence of photovoltaic module electrical performance: a review of efficiency/power correlations” Solar Energy, 2009;83(5):614–24.

[90] Martínez-Moreno F, Muñoz J, Lorenzo E, “Experimental model to estimate shading losses on PV arrays,” Solar Energy Materials and Solar Cells, 2010;94 (12):2298–303.

[91] de Oliveira Reiter RD, Michels L, Pinheiro JR, Reiter RA, Oliveira SVG, Peres A, “Comparative analysis of series and parallel photovoltaic arrays under partial shading conditions,” 10th IEEE/IAS international conference on Industry applications (INDUSCON), 2012.

[92] Alonso-Garcia M, Ruiz J., “Analysis and modelling the reverse characteristic of photovoltaic cells,” Solar Energy Materials and Solar Cells, 2006;90(7):1105–20.

[93] Karatepe E, Boztepe M, Colak M., “Development of a suitable model for characterizing photovoltaic arrays with shaded solar cells,” Solar Energy 2007;81(8):977–92.

[94] Tian H, Mancilla-David F, Ellis K, Muljadi E, Jenkins P., “Determination of the optimal configuration for a photovoltaic array depending on the shading condition,” Solar Energy, 2013;95:1–12.

[95] Silvestre S, Boronat A, Chouder A., "Study of bypass diodes configuration on PV modules," Applied Energy 2009;86(9):1632–40.

[96] Patel H, Agarwal V, Member S., "MATLAB-based modeling to study the effects of partial shading on PV array characteristics," IEEE Transactions Energy Conversion, 2008;23(1):302–10.

[97] Villalva MG, Gazoli JR., "Comprehensive approach to modeling and simulation of photovoltaic arrays," IEEE Transactions on Power Electronics, 2009;24 (5):1198–208.

[98] Storey J, Wilson PR, Bagnall D, "Simulation platform for dynamic photovoltaic arrays," IEEE Energy Conversion Congress and Exposition (ECCE), 2013.

[99] Ramaprabha R, Mathur BL., "A comprehensive review and analysis of solar photovoltaic array configurations under partial shaded conditions," International Journal Photoenergy, no. 0, pp. 1–16, 2012.

[100] Villa LF L, Picault D, Raison B, Bacha S, Labonne A., "Maximizing the power output of partially shaded photovoltaic plants through optimization of the interconnections among its modules," IEEE Journal Photovoltaics, 2012;2(2):154–63.

[101] Roopa P, Rajan S and Vengatesh R., "Performance analysis of PV module connected in various configurations under uniform and non-uniform solar radiation conditions," International conference on recent advancements in electrical, electronics and control engineering (ICONRAEECE), 2011.

[102] Gao L, Dougal RA, Liu S, Iotova AP, "Parallel-connected solar PV system to address partial and rapidly fluctuating shadow conditions," IEEE Transactions on Industrial Electronics, 2009;56(5):1548–56.

[103] Picault D, Raison B, Bacha S, De La Casa J, Aguilera J, Casa JD L., "Forecasting photovoltaic array power production subject to mismatch losses," Solar Energy 2010;84(7):1301–9.

[104] Velasco-Quesada G, Guinjoan-Gispert F, Piquè-Lopez R, Romàn- Lumbreras M, Conesa-Roca A., "Electrical PV array reconfiguration strategy for energy extraction improvement in grid-connected PV systems," IEEE Transactions on Industrial Electronics, 2009;56 (11):431931.

[105] Velasco G, Negroni JJ, Guinjoan F, Pique R., "Energy generation in PV grid-connected systems: power extraction optimization for plant oriented PV generators," IEEE ISIE, June 2005:1025–30.

[106] El-Dein MS, Kazerani M, Salama M., "Optimal total cross tied interconnection for reducing mismatch losses in photovoltaic arrays," IEEE Transactions on Sustainable Energy, 4 (2013) 99.

[107] Romano P, Candela R, Cardinale M, Li Vigni V, Musso D, Sanseverino E Riva., "Optimization of photovoltaic energy production through an efficient switching matrix," Journal of Sustainable Energy, 2013;1(3):227–36.

[108] Wilson P, Storey J, Bagnall D., "Improved optimization strategy for irradiance equalization in dynamic photovoltaic arrays," IEEE Transactions Power Electronics, 2013;28(6):2946–56.

[109] Nguyen DD, Lehman B., "Performance evaluation of solar photovoltaic arrays including shadow effects using neural network," IEEE energy conversion congress and exposition, pp. 3357–62, 2009.

[110] Nguyen D, Lehman B., "An adaptive solar photovoltaic array using model based reconfiguration algorithm," IEEE Transactions Industrial Electronics, 2008;55(7):2644-2654.

[111] Nguyen D, Lehman B., "Modeling and simulation of solar PV arrays under changing illumination conditions," IEEE workshops on computers in power electronics, pp. 295–99, 2006.

[112] Cheng Z, Pang Z, Liu Y, Xue P., "An adaptive solar photovoltaic array reconfiguration method based on fuzzy control," 8th World Congress on intelligent control and automation, pp. 176–81, 2010.

[113] Rani BI, Ilango GS, Nagamani C., "Enhanced power generation from PV array under partial shading conditions by shade dispersion using Su Do Ku configuration," IEEE Transactions on Sustainable Energy, 4(3), pp. 594-601, 2013.

[114] Alahmad M, Chaaban MA, Lau SK, Shi J, Neal J., "An adaptive utility interactive photovoltaic system based on a flexible switch matrix to optimize performance in real-time," Solar Energy, 2012;86(3):951–63.

[115] Chaaban MA, Alahmad M, J Neal, Shi J, Berryman C, Cho Y., "Adaptive photovoltaic system," 36th annual conference on IEEE industrial electronics society, IECON, November 2010, p. 3192–7.

[116] Storey J, Wilson PR, Bagnall D., "The optimized string dynamic photovoltaic array," IEEE Transactions Power Electronics, 2013.

[117] Patnaik B, Sharma P, Trimurthulu E, Duttagupta SP, Agarwal V., "Reconfiguration strategy for optimization of solar photovoltaic array under non-uniform illumination conditions," 37th IEEE photovoltaic specialists conference; June 2011, p. 1859–64.

[118] Patnaik B, Mohod J, Duttagupta SP., "Dynamic loss comparison between fixed state and reconfigurable solar photovoltaic array," 38th IEEE Photovoltaic Specialists Conference (PVSC), pp. 1633-1638, 2012.

[119] dos Santos P, Vicente EM, Ribeiro ER., "Reconfiguration methodology of shaded photovoltaic panels to maximize the produced energy," 11th Brazilian power electronics conference; September 2011, pp.700–706.

[120] dos Santos P, Vicente E. M., Ribeiro ER., "Relationship between the shading position and the output power of a photovoltaic panel," 11th Brazilian Power Electronics Conference; September 2011, pp.676–81.

[121] Firth S, Lomas K, Rees S., "A simple model of PV system performance and its use in fault detection," Solar Energy, April 2010;84(4):624–35.

[122] Oozeki T, Izawa T, Otani K, Kurokawa K., "An evaluation method of PV systems," Solar Energy Materials and Solar Cells, 2003;75(3–4):687–95.

[123] M. Benghanem and A. Maafi, "Data acquisition system for photovoltaic systems performance monitoring," IEEE Trans. Instrum. Meas., 47(1), pp.30–33, Feb. 1998.

[124] X Zou, Bian L, Yonghui Z, Haitao L., "Performance monitoring and test system for grid-connected photovoltaic systems," Proc. of IEEE Power and Energy Engineering Conference (APPEEC), 2012:1-4.

[125] Commission IE. International standard IEC 61724: photovoltaic system performance, IEC 1998.

[126] van Dyk E, Meyer E, Vorster F, Leitch A., "Long-term monitoring of photovoltaic devices," Renewable Energy, 2002;25(2):183–97.

[127] Velasco G, Negroni J., "Irradiance equalization method for output power optimization in plant oriented grid-connected PV generators," Power Electronics Applications, 2005.

[128] Patnaik B., "Distributed multi-sensor network for real time monitoring of illumination states for a reconfigurable solar photovoltaic array," International Symposium on Physics and Technology of Sensors (ISPTS), 2012.

[129] Xiaoli X, Daoe Q., "Remote monitoring and control of photovoltaic system using wireless sensor network," International conference on electric information and control engineering; April 2011. p. 633–8.

[130] E. Dirks, A. Gole, and T. Molinski, "Performance evaluation of a building integrated photovoltaic array using an internet based monitoring system," IEEE Power Engineering Society General Meeting, 2006, pp. 5.

[131] W. Kolodenny, M. Prorok, T. Zdanowicz, N. Pearsall, and R. Gottschalg, "Applying modern informatics technologies to monitoring photovoltaic (PV) modules and systems," 33rd IEEE in Photovoltaic Specialists Conference, PVSC '08, May 2008, pp. 1 –5.

[132] M. Zahran, Y. Atia, A. Al-Hussain, and I. El-Sayed, "Labview based monitoring system applied for PV power station," Proceedings of the 12th WSEAS international conference on Automatic control, modelling & simulation, 2010, pp. 65–70.

[133] Adafruit Learning Systems, Adafruit INA219 Current Sensor Breakout manual.

[134] Maxim Integrated, DS18S20 High-Precision 1-Wire Digital Thermometer Datasheet.

[135] IXYS Corporation, SLMD481H08L IXOLARTM High Efficiency SolarMD Datasheet.

[136] Texas Advanced Optoelectronic Solutions Inc., TSL230BRD Programmable Light-To-Frequency Converters Datasheet.

[137] F. Kasten and A. T. Young, "Revised optical air mass tables and approximation formula," Appl. Opt., vol. 28, no. 22, pp. 4735–4738, Nov 1989.

[138] D. King, J. Kratochvil, and W. Boyson, "Photovoltaic array performance model," Sandia National Laboratory, Tech. Rep., 2004.

[139] W. De Soto, S. Klein, and W. Beckman, "Improvement and validation of a model for photovoltaic array performance," Solar Energy, vol. 80, no. 1, pp. 78 – 88, Aug. 2006.

[140] D. King, "Photovoltaic module and array performance characterization methods for all system operating conditions," in AIP Conference Proceedings. IOP Institute of Physics Publishing ltd., 1997, pp. 347–368.

[141] Introduction to Photovoltaic Systems, Renewable Energy, the Infinite Power of Texas, SECO Fact Sheet No.11.

[142] Solmetric, Application Note PVA-600-1 Guide to Interpreting I-V Curve.

APPENDIX A

ARDUINO CODE

```
//Firmware Code burned onto the Arduino board to transmit all the sensors data to the control PC running LABVIEW.

//Mux Shield for analog inputs

#include <MuxShield.h>

#include <Wire.h>

//Current Sensor

#include <Adafruit_INA219.h>

//Temperature Sensor

#include <OneWire.h>

#include <DallasTemperature.h>

// Data wire is plugged into pin 5 on the Arduino

#define ONE_WIRE_BUS 5

//Initialize the Mux Shield

MuxShield muxShield;

//Arrays to store analog values after recieving them

int IO1AnalogVals[16];

int IO2AnalogVals[16];

int IO3AnalogVals[16];

//Intialize Four Current Sensors

Adafruit_INA219 ina219_A;

Adafruit_INA219 ina219_B(0x41);

Adafruit_INA219 ina219_C(0x44);

Adafruit_INA219 ina219_D(0x45);

// Setup a oneWire instance to communicate with any OneWire devices (not just Maxim/Dallas temperature ICs)

OneWire oneWire(ONE_WIRE_BUS);

// Pass our oneWire reference to Dallas Temperature.

DallasTemperature sensors(&oneWire);

//Variables for Timing and establishing connection

int ledPin=13;
```

```
//   double t = 0;
//   double s = 0;
void setup(void)
{
//Temperatur Reading
// Start up the One Wire And Temperature Sensor Library
sensors.begin(); // IC Default 9 bit. If you have troubles consider upping it 12. Ups the delay giving the IC more time to process the temperature measurement
// call sensors.requestTemperatures() to issue a global temperature
// request to all devices on the bus
sensors.requestTemperatures(); // Send the command to get temperatures
//delay(6000);
//Set I/O 1, I/O 2, and I/O 3 as analog inputs
muxShield.setMode(1,ANALOG_IN);
muxShield.setMode(2,ANALOG_IN);
muxShield.setMode(3,ANALOG_IN);
//CurrentSensing Frequency
uint32_t currentFrequency;
//Current Sensing Begin
ina219_A.begin();// Initialize first board (default address 0x40)
ina219_B.begin();// Initialize second board with the address 0x41
ina219_C.begin();// Initialize second board with the address 0x44
ina219_D.begin();// Initialize second board with the address 0x45
// s=millis();
// start serial port at 115200 bps:
Serial.begin(115200);
digitalWrite(ledPin,HIGH);
//establishContact();  // send a byte to establish contact until receiver responds
digitalWrite(ledPin,LOW);
```

```
Serial.println(sensors.getTempCByIndex(0)); // Why "byIndex"? You can have more than one IC on the same bus. 0 refers to the first IC on the wire}
void loop(void)
{float current_mA_A = 0;
float current_mA_B = 0;
float current_mA_C = 0;
float current_mA_D = 0;
current_mA_A = ina219_A.getCurrent_mA();
current_mA_B = ina219_B.getCurrent_mA();
current_mA_C = ina219_C.getCurrent_mA();
current_mA_D = ina219_D.getCurrent_mA();
//Current values
for (int i=0; i<13; i++)
{
Serial.print(float(muxShield.analogReadMS(1,i)*4.96 / 1023));
Serial.print(" ");}
Serial.print(current_mA_A);Serial.print(" ");
Serial.print(current_mA_B);Serial.print(" ");
Serial.print(current_mA_C);Serial.print(" ");
Serial.println(current_mA_D);}
//Code For Establishing Connection with the COM port
void establishContact() {
while (Serial.available() <= 0) {
Serial.println('B');   // send a capital A
delay(100);}}
```